Published in final edited form as:

Structure. 2023 July 06; 31(7): 836–847.e6. doi:10.1016/j.str.2023.05.001.

Dual Mechanisms of Cholesterol-GPCR Interactions That Depend on Membrane Phospholipid Composition

Arka Prabha Ray[1,†], **Naveen Thakur**[1,†], **Niloofar Gopal Pour**[1], **Matthew T. Eddy**[1,*]

[1]Department of Chemistry, University of Florida, 126 Sisler Hall, Gainesville, FL 32611, USA

SUMMARY

Cholesterol is a critical component of mammalian cell membranes and an allosteric modulator of G protein-coupled receptors (GPCRs), but divergent views exist on the mechanisms by which cholesterol influences receptor functions. Leveraging the benefits of lipid nanodiscs, i.e., quantitative control of lipid composition, we observe distinct impacts of cholesterol in the presence and absence of anionic phospholipids on the function-related conformational dynamics of the human A_{2A} adenosine receptor (A_{2A}AR). Direct receptor-cholesterol interactions drive activation of agonist-bound A_{2A}AR in membranes containing zwitterionic phospholipids. Intriguingly, the presence of anionic lipids attenuates cholesterol's impact through direct interactions with the receptor, highlighting a more complex role for cholesterol that depends on membrane phospholipid composition. Targeted amino acid replacements at two frequently predicted cholesterol interaction sites showed distinct impacts of cholesterol at different receptor locations, demonstrating the ability to delineate different roles of cholesterol in modulating receptor signaling and maintaining receptor structural integrity.

Graphical Abstract

*Correspondence: matthew.eddy@chem.ufl.edu.

AUTHOR CONTRIBUTIONS

A.P.R., N.T., and N.G.P. performed protein production, purification, and nanodisc sample preparation. N.G.P. carried out molecular cloning. A.P.R. and N.T. recorded NMR data, ligand binding data, and fluorescence data with input from M.T.E. A.P.R., N.T. and M.T.E. analyzed NMR data. M.T.E., A.P.R. and N.T. wrote the manuscript with input from all authors.

†These authors contributed equally to this work

Lead Contact: Matthew Eddy

DECLARATION OF INTERESTS

The authors declare no competing interests.

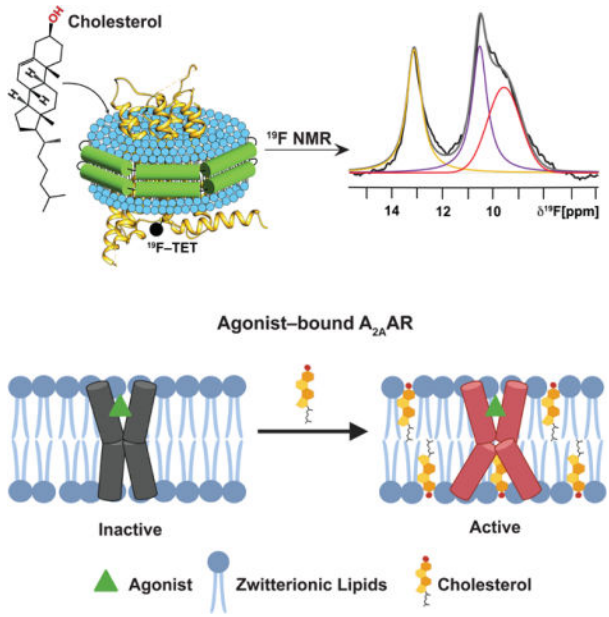

eTOC Blurb

Ray and Thakur et al. use ^{19}F-NMR to observe how cholesterol affects the conformational equilibria of the A_{2A} adenosine receptor. The impact of cholesterol varies depending on the type of phospholipids present and differs at different receptor locations, affecting either structural stability or receptor signaling activity.

INTRODUCTION

Cholesterol is a major component of mammalian cell membranes and an important regulator of the functions of membrane proteins, as documented extensively in the literature.[1–9] Alterations in cholesterol distribution and metabolism, either through genetic or environmental causes, are highly correlated with numerous health disorders, including Alzheimer's disease,[10] heart disease,[11] and diabetes.[12] Cholesterol is also increasingly known for its role as an allosteric modulator of G protein-coupled receptors (GPCRs), integral membrane sensory proteins, and targets of over 35% of FDA-approved drugs.[13]

Literature data have reported the impacts of cholesterol on essentially every aspect of GPCR pharmacology and biology.[14–19] Cholesterol has been shown experimentally to act as an allosteric modulator of GPCRs, altering the binding affinities of orthosteric ligands, as observed with, for example, the oxytocin receptor,[20] CXCR4 chemokine receptor,[21] serotonin$_{1A}$ receptor,[22] cannabinoid CB1 receptor[23] and CCR5 chemokine receptor.[24] Structural and biochemical evidence also support the role of cholesterol as a direct orthosteric agonist for some GPCRs, including the smoothened receptor (SMO).[25] In addition to cholesterol's impacts on receptor pharmacology, experimental and computational studies have identified roles of cholesterol in GPCR oligomerization,[26–29] receptor sorting and trafficking,[30–33] and formation of signaling complexes.[19,34,35]

Three general mechanisms have been proposed to understand the influence of cholesterol on GPCR function: direct cholesterol-GPCR interactions, indirectly via modulation of bulk membrane properties, or a combination of both.[36] Support for direct receptor-cholesterol interactions has come, in part, from the observation of cholesterol or cholesterol analogs closely associated with the transmembrane regions of more than 60 GPCRs in X-ray crystallography and cryo-electron microscopy structures, as reviewed.[37] NMR studies of the β_2-adrenergic receptor (β_2AR) indicated that the receptor showed a specific preference to associate with cholesterol over ergosterol,[38] and high-pressure NMR studies reported the cholesterol analog, cholesteryl hemisuccinate (CHS), specifically associated with the β_1-adrenergic receptor (β_1AR) to inhibit its activation.[39] However, there is no consensus on the extent to which specific cholesterol-receptor interactions influence the function of GPCRs, and earlier studies of rhodopsin reported evidence for the influence of cholesterol on rhodopsin function both through direct interactions with rhodopsin[40] and by modulating the properties of the lipid bilayer.[41]

We investigated the mechanism by which cholesterol modulates the function-related dynamics of the human A_{2A} adenosine receptor (A_{2A}AR), a class A GPCR. A_{2A}AR is a model receptor for investigating mechanisms underlying GPCR signaling phenomena, owing to a large number of structures[42–46] and the availability of spectroscopic data in different membrane mimetics.[47–53] A_{2A}AR is an important and validated drug target for Parkinson's disease[54] and cancers[55] for which cholesterol may play a role. A growing body of literature has documented the impact of cholesterol on A_{2A}AR signaling and pharmacology, though there is no consensus on the precise role of cholesterol or mechanisms by which cholesterol may influence A_{2A}AR function. In HEK293 cells treated with methyl-β-cyclodextrin (MβCD) to deplete cholesterol, A_{2A}AR signaling was observed to significantly decrease,[56] indicating cholesterol was required to achieve a maximum signaling response to agonist stimulation. In a separate study, treatment of C6 glioma cells with MβCD showed an increase in the specific binding of an A_{2A}AR antagonist, suggesting cholesterol inhibited antagonist binding.[15] Canonical cholesterol recognition motifs and cholesterol-binding "hotspots" have been predicted for A_{2A}AR as evidence for specific receptor-cholesterol interactions.[57–59] In contrast to this view, ^{19}F-NMR experiments with A_{2A}AR labeled at position V229C on transmembrane helix 6 concluded cholesterol was a weak positive allosteric modulator and impacts of cholesterol were likely due more to cholesterol-mediated changes in membrane bilayer fluidity rather than direct interactions.[60]

To reconcile these divergent views, we integrated ^{19}F-NMR data with correlative functional and pharmacological assays to investigate the impact of cholesterol on signaling-related A_{2A}AR conformational dynamics. We leveraged the benefits of lipid nanodiscs to quantitatively control lipid composition in all samples. By systematically exploring a wider range of lipid compositions than previously studied, we observed evidence for both the direct and indirect influence of cholesterol. The mechanism of cholesterol influence depended both on the presence of cholesterol and the composition of phospholipids in the membrane. Using conditions where we observe specific cholesterol-receptor interactions, we explored variations in the cholesterol chemical scaffold to test the extent to which cholesterol-A_{2A}AR interactions depended on the structural details of cholesterol molecules. The same conditions also allowed us to investigate two of the most frequently predicted

cholesterol interaction sites.[61–63] Our findings reveal a clear and significant impact of cholesterol on the activation of agonist-bound $A_{2A}AR$ in nanodiscs that contain zwitterionic lipids. This effect is observable even for samples containing only 1–2 molecules of cholesterol per nanodisc. An investigation of cholesterol analogs also yielded comparable results. Interestingly, this response is obscured when $A_{2A}AR$ is embedded in nanodiscs containing mixtures of zwitterionic and anionic lipids, suggesting a potential interplay between anionic lipids and cholesterol. These results are discussed in the context of integrating *in vitro* and *in vivo* data to provide a more comprehensive understanding of the role of cholesterol in GPCR activation mechanisms.

RESULTS

Cholesterol manifests different impacts on the pharmacology of $A_{2A}AR$ antagonists and agonists

For biophysical and functional experiments, a variant of human $A_{2A}AR$ containing a single cysteine replacement at position 289 located at the intracellular surface of helix 7 (Figure S1), $A_{2A}AR$[A289C], was expressed in *Pichia pastoris* using previously described protocols.[64] The location of the introduced cysteine was selected based on literature data from ^{19}F NMR studies of $A_{2A}AR$, which demonstrated NMR spectra of $A_{2A}AR$ labeled with ^{19}F-2,2,2-trifluoroethanethiol at this position were sensitive to differences in the efficacies of bound ligands.[51] This position was also shown to be sensitive to modulation of the $A_{2A}AR$ conformational ensemble by membrane phospholipids.[64] C289 was the only cysteine available for chemical conjugation, as previously demonstrated.[51]

To investigate the role of cholesterol on the conformational equilibria of $A_{2A}AR$, we prepared samples of $A_{2A}AR$[A289C] in lipid nanodiscs containing binary mixtures of POPC (1-palmitoyl-2-oleoyl-glycero-3-phosphocholine) and cholesterol, or ternary mixtures of POPC and POPS (1-palmitoyl-2-oleoyl-sn-glycero-3-phospho-L-serine) and cholesterol, or POPC and POPG (1-palmitoyl-2-oleoyl-sn-glycero-3-phospho-(1'-rac-glycerol)) and cholesterol, where the amount of cholesterol was varied from 0 to 15 mol%. We observed homogenous preparations could be achieved for nanodiscs containing up to 15 mol% cholesterol and attempts to prepare nanodiscs with more resulted in heterogeneous, aggregated samples. This is consistent with analogous observations described previously, which reported higher concentrations of cholesterol inhibited nanodisc formation, possibly due to increased membrane rigidity.[60,65,66] We therefore focused our study on membrane compositions containing ≤15 mol% cholesterol. While this is lower than what has been observed in some mammalian cell membranes,[67] this amount still allowed us to investigate possible mechanisms of cholesterol influence on $A_{2A}AR$.

To obtain homogeneous lipid compositions in nanodiscs, mixtures of lipids were quantitatively weighed and dissolved in chloroform, dried down to form a thin film, and then reconstituted in buffer (STAR Methods). Analytical size exclusion chromatography characterization of purified lipid nanodiscs containing $A_{2A}AR$, phospholipids, and varying amounts of cholesterol showed monodispersed and homogeneous samples (Figure S2). The phospholipid composition of nanodisc samples containing $A_{2A}AR$ was verified by ^{31}P-NMR, which showed the relative amounts of each phospholipid species in the nanodisc

samples quantitatively agreed with the intended amounts (Figure S3). The amount of cholesterol in each nanodisc sample was verified using the Amplex Red Cholesterol Assay, a fluorometric method for the enzymatic detection of cholesterol[68], and confirmed to be consistent with targeted amounts (Table S1). We also note that this assay has been used to quantify concentrations of other sterols including ergosterol[69], which is produced by *P. pastoris*. Using the fluorometric assay we did not detect the presence of other sterols in nanodisc samples that were not prepared by purposely adding sterols. To confirm the receptor was folded in all employed lipid compositions, we recorded fluorescence thermal shift assays using a thiol-reactive dye, N-[4-(7-diethylamino-4-methyl-3-coumarinyl)phenyl]maleimide (CPM), for A_{2A}AR[A289C] in complex with the full agonist 5'-*N*-ethylcarboxamidoadenosine (NECA). As the nanodisc scaffold protein MSP1D1 contains no cysteines, the assay thus observed a direct response of the thermal unfolding of the receptor. A_{2A}AR was folded in all studied lipid compositions across the full range of cholesterol concentrations (Figure S4). We observed at most a minimal impact of cholesterol on the measured melting temperature of A_{2A}AR[A289C] for nanodisc samples prepared either with POPC and cholesterol or ternary mixtures of POPC, POPS, and cholesterol (Figure S4). The more significant impact was the presence or absence of POPS, consistent with earlier studies.[64]

To investigate the impact of cholesterol on the pharmacological activity of A_{2A}AR, we measured affinities for the antagonist ZM241385 and agonist NECA with radioligand competition binding experiments in lipid nanodiscs containing variable amounts of cholesterol. For all samples studied, we observed clear evidence of ligand binding, indicating A_{2A}AR[A289C] retained pharmacological activity across the range of cholesterol concentrations used in subsequent NMR experiments (Figure 1). For experiments with the antagonist ZM241385, we measured at most a factor of ~3 difference in binding affinities in samples containing 0 to 10 mol% cholesterol, with no clear relationship between the amount of cholesterol and determined K_D value for the antagonist (Figure 1A and Table S2), suggesting these relatively smaller differences were likely unrelated to the amount of cholesterol present. For the agonist NECA, we observed a difference of ~4.5 in measured binding affinities between samples containing 0 mol% cholesterol and 10 mol% cholesterol, with a linear decrease in the agonist dissociation constant with increasing amounts of cholesterol (Figure 1B and Table S2). This suggested a potential correlation between the presence of cholesterol and affinity for agonists, though less than an order of magnitude difference in agonist affinities between samples containing 0 to 10 mol% cholesterol.

Cholesterol is required to populate an active A_{2A}AR ensemble in zwitterionic phospholipid membranes

We investigated the impact of cholesterol on the function-related conformational dynamics of A_{2A}AR by NMR using a ^{19}F-NMR reporter group introduced at position C289, located in transmembrane helix 7, with 2,2,2-trifluoroethanethiol (TET) covalently attached *via* an in-membrane chemical modification approach,[70] yielding A_{2A}AR[A289C^{TET}]. Earlier studies demonstrated no other cysteines were available for ^{19}F-labeling.[51] The ^{19}F-NMR reporter at position C289 was shown to be highly sensitive to function-related changes

in the efficacies of bound drugs[51] and changes in membrane phospholipid composition,[64] providing 'fingerprints' for the corresponding functional states.

We recorded ^{19}F-NMR spectra of A_{2A}AR[A289C^{TET}] in complex with the antagonist ZM241385 in lipid nanodiscs containing POPC and either without cholesterol or with 5 mol% cholesterol (Figure 2A). For both samples, highly similar spectra were observed containing two components, labeled P1 and P3, with P3 being the dominant component in the spectrum. In earlier studies, ^{19}F-NMR spectra of antagonist-bound A_{2A}AR[A289C^{TET}] in DDM/CHS micelles,[51] P3 had been assigned to an inactive conformation of the receptor and P1 had been observed for both antagonist-bound and agonist-bound A_{2A}AR[A289C^{TET}].[51] The spectra of antagonist-bound A_{2A}AR[A289C^{TET}] shown in Figure 2A are also highly similar to spectra reported of antagonist-bound A_{2A}AR[A289C^{TET}] in lipid nanodiscs of binary mixtures of phospholipids that did not contain cholesterol.[64] The chemical shifts for components P1 and P3 appear to be highly similar for preparations of antagonist-bound A_{2A}AR[A289C^{TET}] either in DDM/CHS micelles[51] or lipid nanodiscs without cholesterol.[64] Further, only relatively smaller variations in the relative intensities of components P1 and P3 were observed in the absence and presence of cholesterol for antagonist-bound A_{2A}AR (Figure 2A), compared with more striking changes observed for agonist-bound A_{2A}AR[A289C^{TET}] upon addition of cholesterol (see below). Specifically, for antagonist-bound A_{2A}AR[A289C^{TET}] we observed a ~15% decrease in the relative population for state P3 and a ~30% increase in the population of state P1 upon addition of cholesterol (Table S4). The dominant component in the spectrum was still clearly P3, indicating the inactive conformational ensemble remained similar in the absence and the presence of cholesterol.

In contrast to our observations with antagonist-bound A_{2A}AR, ^{19}F-NMR spectra of agonist-bound A_{2A}AR[A289C^{TET}] showed a striking dependence on the presence of cholesterol. ^{19}F-NMR spectra of A_{2A}AR[A289C^{TET}] in complex with the agonist NECA in lipid nanodiscs containing POPC were highly similar to spectra of A_{2A}AR[A289C^{TET}] in complex with the antagonist ZM241385 (Figure 2B). This indicated we observed an inactive A_{2A}AR conformational ensemble even with a saturating amount of agonist present, consistent with earlier studies in nanodiscs containing only zwitterionic phospholipids.[64] From the radioligand binding data in Figure 1, we concluded the pharmacological activity of A_{2A}AR was preserved in the employed lipid composition, and thus the observation of the inactive conformational ensemble was not due to impaired ligand binding.

Compared to the results in nanodiscs containing only POPC, we observed a clear-cut response to cholesterol for agonist-bound A_{2A}AR[A289C^{TET}] in nanodiscs containing POPC. ^{19}F-NMR spectra of agonist-bound A_{2A}AR in nanodiscs containing POPC and 0.5 mol% cholesterol showed the hallmarks of an active ensemble, noted by the disappearance of peak P3 and the emergence of two new peaks P2 and P4 (Figure 2B), which had highly similar chemical shifts to signals identified for agonist-bound A_{2A}AR in DDM/CHS micelles.[51] Previously, we assigned P4 to the fully active A_{2A}AR conformation by carefully examining experimental conditions in which we observed a population of P4 only upon complex formation of A_{2A}AR[A289C^{TET}] with mini-G_S.[64] The composition of 0.5 mol% cholesterol corresponds on average to 1 to 2 molecules of cholesterol per nanodisc (see

Discussion), which was verified in fluorometric assays as described above. At this relatively low concentration of cholesterol, we did not anticipate cholesterol would have a significant impact on membrane fluidity, which may also potentially impact A_{2A}AR. To verify this, we recorded fluorescence spectra of nanodiscs containing POPC, varying amounts of cholesterol, and the lipophilic fluorescent probe Laurdan, which is a sensitive probe of membrane fluidity.[71] We observed that nanodiscs containing 0.5 mol% cholesterol showed almost identical membrane phase behavior compared with nanodiscs containing only POPC (Figure S5). Based on these collective observations, we concluded the effects of cholesterol observed on populating the active state ensemble of agonist-bound A_{2A}AR must be due to a direct influence on the receptor rather than to the modulation of the bulk properties of the membranes in the nanodiscs.

We recorded additional ^{19}F-NMR spectra of agonist-bound A_{2A}AR[A289C^{TET}] in nanodiscs containing POPC and 5 mol% cholesterol or 10 mol% cholesterol. The fits for the data for all spectra were evaluated by calculating the residual difference between the raw data and the sum of the individually fit components (Figure S6), from which we conclude that no new signals were observed from earlier studies of A_{2A}AR in DDM/CHS[51] or in lipid nanodiscs.[64] The ^{19}F-NMR spectrum of agonist-bound A_{2A}AR[A289C^{TET}] in nanodiscs containing POPC and 5 mol% cholesterol qualitatively resembled the spectrum for A_{2A}AR in nanodiscs containing 0.5 mol% cholesterol with marginally reduced linewidths observed for states P4 and P2 (Figure 2B), possibly indicating reduced conformational plasticity with a higher concentration of cholesterol. While the ^{19}F-NMR spectrum A_{2A}AR[A289C^{TET}] in nanodiscs containing POPC and 10 mol% cholesterol qualitatively resembled spectra with lower amounts of cholesterol, we observed a slightly diminished intensity for state P4 (Figure 2B). In the membrane fluidity measurements with Laurdan, we observed a reduction in membrane fluidity with increasing amounts of cholesterol. Samples prepared with 10 mol% cholesterol showed the largest increase in order (Figure S5). This observation may correlate with the slightly diminished intensity for state P4 observed with increasing cholesterol concentration. We also recorded ^{19}F-NMR spectra at a higher temperature of 300 K of A_{2A}AR[A289C^{TET}] in complex with NECA in nanodiscs containing POPC and either 0.5 mol% cholesterol or 5 mol% cholesterol (Figure S7). At 300 K, we observed a ~50% increase in the popultion of state P4 with respect to the total integrated spectrum (Table S4). We anticipate that at even higher temperatures we would likely observe additional marginal increases in the population of P4.

Cholesterol analogs also significantly influence the conformational equilibria of agonist-bound A_{2A}AR

Having established experimental conditions where we observed a clear impact of cholesterol on populating the active ensemble of agonist-bound A_{2A}AR, we investigated whether this impact was specific to cholesterol or could be observed also with other sterols. Cholesterol-protein interactions are thought to be nuanced, and it has been proposed that details of the chemical structure of cholesterol facilitate its interactions with membrane proteins. MD simulations have predicted that specific structural features of cholesterol molecules form unique interactions with membrane proteins at cholesterol interaction sites.[56–59,72] We recorded ^{19}F-NMR spectra of A_{2A}AR[A289C^{TET}] in complex with the

agonist NECA in lipid nanodiscs containing POPC and 0.5% mol fraction of one of three different sterols: epicholesterol, ergosterol, or digoxigenin (Figure 3). The three sterols were chosen to explore the extent to which the influence of cholesterol on the conformational ensemble of $A_{2A}AR$ depended on specific features of the cholesterol chemical structure, as epicholesterol is an enantiomer and ergosterol is a diastereomer of cholesterol. ^{19}F-NMR spectra of agonist-bound $A_{2A}AR[A289C^{TET}]$ in the presence of POPC and 0.5 mol% of epi-cholesterol, ergosterol, or digoxigenin were similar to spectra recorded in the presence of 0.5 mol% cholesterol, showing an active state ensemble (Figure 3 and Figure S8). The relative population of state P4 varied among the spectra recorded with different sterols, with the sample prepared with digoxigenin showing the lowest relative population of P4 and the sample prepared with epicholesterol showing approximately twice the relative population (Table S4). Despite these variations, there was a distinct difference in the overall spectral fingerprint of all samples prepared with 0.5 mol% sterol compared to agonist-bound receptor in the absence of cholesterol. These observations suggest the influence of cholesterol on the $A_{2A}AR$ conformational ensemble does not depend on specific details of the cholesterol chemical scaffold.

Anionic phospholipids modulate the impact of cholesterol on the $A_{2A}AR$ conformational equilibria

In a previous study, we showed that the presence of anionic lipids, including POPS and POPG, modified the conformational equilibrium of agonist-bound $A_{2A}AR$.[64] Our findings revealed that ^{19}F-NMR spectra exhibited an inactive conformational ensemble for agonist-bound $A_{2A}AR[A289C^{TET}]$ in nanodiscs containing zwitterionic lipids. Upon the introduction of anionic phospholipids, an active conformational ensemble was observed.[64] It was therefore of interest to investigate how the $A_{2A}AR$ conformational equilibria were affected by ternary mixtures of zwitterionic phospholipids, anionic phospholipids and cholesterol. We prepared samples of $A_{2A}AR$ reconstituted into nanodiscs containing POPC, 5 mol% cholesterol, and either POPS (1-palmitoyl-2-oleoyl-sn-glycero-3-phospho-L-serine) or POPG (1-palmitoyl-2-oleoyl-sn-glycero-3-phospho-(1'-rac-glycerol)). ^{19}F-NMR spectra of the $A_{2A}AR[A289C^{TET}]$ complex with the antagonist ZM241385 were highly similar in the presence and absence of 5 mol% cholesterol, showing slightly narrower lines in the presence of cholesterol with no significant changes in the relative populations of observed signals (Figure 4A, Figure S9, and Table S4). For agonist-bound $A_{2A}AR$, in contrast to our observations with nanodiscs containing POPC and cholesterol, we observed at most subtle dependence on the presence of cholesterol in ^{19}F-NMR spectra of $A_{2A}AR[A289C^{TET}]$ in nanodiscs containing ternary mixtures of POPC and POPS and cholesterol or POPC and POPG (Figures 4B and 4C). In all cases, we observed the signature of an active ensemble with only subtle changes in the relative populations of P4, P2, and P1 (Figures 4B and 4C, Table S4). ^{19}F-NMR spectra of $A_{2A}AR[A289C^{TET}]$ in nanodiscs containing ternary mixtures of POPC and POPS exhibited a ~20% decrease in the relative population of state P2 upon addition of 5 mol% cholesterol whereas the population of state P1 remained nearly unchanged (Table S4). ^{19}F-NMR spectra of $A_{2A}AR[A289C^{TET}]$ in nanodiscs containing ternary mixtures of POPC and POPG exhibited a ~50% decrease in the population of state P2 upon addition of 5 mol% cholesterol and the population of P1 increased by ~65% (Table S4). ^{19}F-NMR spectra of agonist-bound $A_{2A}AR[A289C^{TET}]$ in nanodiscs containing

a smaller amount of anionic lipids (POPC:POPG, 93:7 molar ratio) also show a diminished effect of the addition of cholesterol (Figure S10) as compared to spectra measured with cholesterol in nanodiscs containing only POPC. We observed an increase by ~20% in the population of state P4, a ~20% reduction in the population of state P2, and the relative population of state P1 remained nearly the same (Table S4).

We further explored the impact of cholesterol on A_{2A}AR function in binary and ternary mixtures of phospholipids by observing the impact of cholesterol and anionic lipids on A_{2A}AR-catalyzed nucleotide exchange using a GTP hydrolysis assay[73] (Figure S11 and Table S3). This assay monitors the exchange of GTP for GDP bound to the stimulatory G protein $G\alpha_S$ upon complex formation with A_{2A}AR[A289C]. In lipid nanodiscs containing POPC, we observed a significant increase in GTPase activity for agonist-bound A_{2A}AR over antagonist-bound A_{2A}AR, as expected (Figure S11). We observed a statistically significant increase in GTPase activity for agonist-bound A_{2A}AR in nanodiscs containing 0.5 mol% cholesterol (Figure S11). A further increase in GTPase activity was observed for A_{2A}AR in nanodiscs containing 5 mol% cholesterol. In nanodiscs containing POPC and 10 mol% cholesterol, activity was still present but appeared to be decreased compared with nanodiscs containing 0.5 and 5 mol% cholesterol. This observation appears consistent with our NMR data showing an active-state ensemble with a lower P4 population for nanodiscs containing 10 mol% cholesterol, as discussed above (Figure 2 and Table S4), which may reflect an impact of the decrease in membrane fluidity on the A_{2A}AR conformational ensemble. In nanodiscs containing mixtures of POPC and POPS, the addition of anionic lipids correlated with a significant increase in GTPase activity for agonist-bound A_{2A}AR (Figure S11), consistent with our earlier observations of the impact of anionic phospholipids on populating an A_{2A}AR active state ensemble.[64] For binary phospholipid compositions, the presence of cholesterol showed a positive impact on GTPase activity; however, the impact of cholesterol was significantly muted in the presence of anionic lipids compared with the GTPase activity of A_{2A}AR in nanodiscs containing only zwitterionic lipids, which correlated with the corresponding ^{19}F-NMR spectra (Figure 4, Table S4).

Distinct roles for different cholesterol interaction sites influence signaling and receptor stability

Sequence analysis and structure-based computational modeling have identified several putative sites for cholesterol interactions with A_{2A}AR, described as cholesterol recognition amino acid consensus (CRAC) sequences or cholesterol consensus motifs (CCM). One CCM site predicted for A_{2A}AR from all-atom simulation data[74] involved residues Y43$^{2.41}$, S47$^{2.45}$, K122$^{4.44}$, I125$^{4.46}$ and W129$^{4.50}$ (superscripts indicate the Ballesteros-Weinstein nomenclature[75]). This location has also been proposed to be a cholesterol interaction site in other class A GPCRs, including the β_2AR.[76] Amino acid replacement of these residues in A_{2A}AR resulted in reduced ligand specific binding and reduced cAMP signaling in HEK293 cells.[61] Additional cholesterol interaction sites were observed in molecular dynamics simulations, including a location at the intracellular surface between TMVI and TMVII[62] involving R291$^{7.56}$ (Figure 5A). From our earlier results showing the involvement of R291 in facilitating A_{2A}AR interactions with anionic lipids,[64] we sought to test if this

residue was also important for mediating the effects of cholesterol on the A_{2A}AR active-state conformational ensemble.

We selected W129 and R291 for amino acid replacement to test if the variants A_{2A}AR[A289C,R291Q] and A_{2A}AR[A289C,W129I] showed evidence for disrupting cholesterol-A_{2A}AR interactions. W129 was replaced with isoleucine to disrupt potential ring stacking between cholesterol and A_{2A}AR, and R291 was replaced with the relatively shorter, uncharged amino acid glutamine to potentially alter interactions with the cholesterol 3β-hydroxyl group, which orients cholesterol to the membrane surface. ^{19}F-NMR spectra of agonist complexes with the A_{2A}AR variants A_{2A}AR[A289C^{TET},R291Q] and A_{2A}AR[A289C^{TET},W129I] were recorded using conditions we had previously identified where a clear response to cholesterol was observed for agonist-bound A_{2A}AR in nanodiscs containing POPC and 0.5 mol% cholesterol (1–2 cholesterol molecules per nanodisc) (Figure 2). ^{19}F-NMR spectra of agonist-bound A_{2A}AR[A289C^{TET},R291Q] in nanodiscs containing POPC and 0.5 mol% cholesterol showed the spectral signature of an active-state ensemble but with a significant decrease in the population of the active-state P4 (Figure 5B). We had previously shown that pharmacological activity was preserved for this variant and ^{19}F-NMR spectra of agonist-bound A_{2A}AR[A289C^{TET},R291Q] in lipid nanodiscs containing only POPC resembled an inactive conformational ensemble.[64] We had also shown that the R291Q amino acid replacement increased the basal activity of the receptor, manifesting in the ^{19}F-NMR spectra of A_{2A}AR[A289C^{TET},R291Q] as an increased population of the state P4.[64] The presence of 0.5 mol% cholesterol did populate an active ensemble but with a reduced impact, which suggests that this site may contribute toward the impact of cholesterol in addition to one or more other locations. Thus, in the present study it is remarkable that the relative population of P4 is observed to be decreased for A_{2A}AR[A289C^{TET},R291Q] in conditions where we observe a much larger population for P4 for A_{2A}AR[A289C^{TET}]. ^{19}F-NMR spectra of agonist bound A_{2A}AR[A289C^{TET},W129I] in nanodiscs containing POPC and 0.5 mol% cholesterol also showed an altered conformational equilibria with changes in the relative populations of states P1 and P2 (Figure 5C), with an increase in the population of P1 by ~60% and a decrease in the population of P2 by a factor of 5–6 (Table S4). However, we observed a significant population for state P4 similar to the observations with A_{2A}AR[A289C^{TET}], indicating the presence of a substantial active state population. The distinct ^{19}F-NMR spectra of the agonist complexes with A_{2A}AR[A289C^{TET},R291Q] and A_{2A}AR[A289C^{TET},W129I] in the presence of 0.5 mol% cholesterol suggest potentially different roles for cholesterol interactions in the two locations.

DISCUSSION

The pharmacological data in Figure 1 show no correlation between measured binding affinities for antagonists and cholesterol and a potential positive correlation between binding affinities of agonists and cholesterol concentrations in lipid nanodiscs, albeit less than a factor of 10 over the range of cholesterol concentrations studied. Previous studies reported an increase in specific binding of the antagonist ZM241385 to A_{2A}AR upon using MβCD to remove cholesterol from C6 glioma cells.[15] As our pharmacological data were recorded for A_{2A}AR in lipid nanodiscs, it suggests the observations in glioma cells may reflect a more

complicated interplay between cholesterol and additional membrane lipids in the cellular environment that could impact A_{2A}AR pharmacology.

In nanodiscs containing POPC, ^{19}F-NMR spectra of agonist-bound A_{2A}AR showed a clear response to the presence of just 1–2 molecules cholesterol per nanodisc (Figure 2). There was no observable impact of this relatively lower amount of cholesterol on the fluidity of the membranes in nanodiscs (Figure S5). We concluded the impact of cholesterol on the A_{2A}AR conformational ensemble was due to direct interactions with the receptor. The estimation of 0.5 mol% cholesterol corresponding to 1 to 2 molecules of cholesterol, on average, was based on both experimental data presented in this study and earlier computational studies that estimated the number of lipid molecules in each nanodisc. In the ^{19}F-NMR spectra of agonist-bound A_{2A}AR in nanodiscs containing POPC and 0.5 mol% cholesterol, there is no observable population of state P3 (Figure 2B), whereas in the absence of any cholesterol, the signal for P3 is clearly observed as the most intense signal in the spectrum (Figure 2A). These results indicate that for samples prepared with 0.5 mol% cholesterol, nearly all nanodiscs must contain at least 1 molecule of cholesterol, and the number of nanodiscs that do not contain cholesterol is below the detection limit of the experiment. Therefore, the NMR data provide a lower limit for the number of molecules of cholesterol per nanodisc. Previous attempts to estimate the number of lipid molecules in nanodiscs relied mainly on computational approaches, including those by Denisov and coworkers[77], which estimated the number of lipid molecules in nanodiscs made from the MSP1D1 scaffold protein to range between 112 and 160 in multiple simulations.[77] However, these simulations were acknowledged to have limitations, including the lack of an experimental structure of MSP1D1 in its nanodisc state and challenges in accurately modeling the flexibility and deformations of the scaffold protein that are anticipated to be observed for real samples. Additionally, simulations have considered systems containing a single lipid component and did not consider the role of cholesterol or compositions of multiple lipid types.[77] Based on our experimental data, we estimate that the number of lipid molecules per nanodisc is likely closer to the upper end of the previously estimated range, and may even somewhat exceed this range in the specific conditions employed in our experiments.

The NMR observations from Figure 2 aligned with our GTP hydrolysis assay results, which showed a positive correlation of nucleotide exchange for nanodiscs containing cholesterol (Figure S11). These observations also appear qualitatively consistent with A_{2A}AR cell signaling experiments, which showed a positive correlation of cAMP production and the presence of cholesterol in membranes.[56] The ^{19}F-NMR data of Figure 2 showed a very different response of A_{2A}AR to cholesterol than what has been reported in previous ^{19}F-NMR studies of A_{2A}AR with an NMR probe in helix VI in nanodiscs containing a mixture of POPC and POPG (3:2 molar ratio).[60] In this earlier study, much more subtle changes were observed in the ^{19}F-NMR spectra between samples in nanodiscs without and with cholesterol, which, combined with additional data from the same study, supported the view that the impact of cholesterol on A_{2A}AR was more likely through modulation of membrane fluidity rather than direct interactions with A_{2A}AR.[60] The more subtle changes in the ^{19}F-NMR spectra with and without cholesterol from this earlier NMR study do appear more in line with our observations of A_{2A}AR in nanodiscs containing ternary mixtures of POPC, cholesterol, and either POPS or POPG, where we could not distinguish the impact

of cholesterol from that of anionic lipids (Figure 4). Indeed, in the presence of just 7 mol% POPG, one could no longer distinguish potential effects of cholesterol from those of the presence of anionic lipids on the agonist-bound A_{2A}AR conformational ensemble (Figure S10). Taken together with earlier spectroscopic and signaling studies, this suggests the mechanism of cholesterol's influence on A_{2A}AR depends on the phospholipid composition of the membrane system used in experiments. A corollary from this conclusion is that for *in vivo* experiments, a full understanding of the impact of cholesterol on receptor function may also require a more complete inventory of the phospholipid composition of cellular membranes, especially if the profile of phospholipids changes upon the addition or depletion of cholesterol.

The presented data interpreted within the context of previous studies suggest cholesterol and anionic lipids may have interchangeable roles in populating an active conformational ensemble for agonist-bound A_{2A}AR (Figure 6). Anionic lipids and cholesterol may also compete for similar locations of interaction with A_{2A}AR. Molecular dynamics simulations observed the displacement of cholesterol by the anionic lipid phosphatidylinositol 4,5-bisphosphate (PIP2) from the A_{2A}AR intracellular surface between helices VI and VII involving interactions with R291.[63] ^{19}F-NMR spectra of agonist-bound A_{2A}AR[A289C^{TET},R291Q] in nanodiscs containing POPC and 0.5 mol% cholesterol showed a significantly diminished impact of cholesterol on the active state conformational ensemble (Figure 5). We had previously shown this residue was also involved in facilitating receptor interactions with anionic lipids.[64]

Cholesterol is observed to associate with receptors at multiple locations in the majority of GPRC crystal and cryo-EM structures,[14,72] and it remains an open question whether potential cholesterol interaction sites can be assigned to different roles. In A_{2A}AR, while mutation of R291Q resulted in diminished impact of cholesterol on the active state conformational ensemble, mutation of a second predicted cholesterol interaction site, W129, resulted in changes to the relative populations of populations P1 and P2 but did not significantly perturb the active-state population P4 (Figure 5 and Table S4). Earlier *in vivo* studies demonstrated the W129 mutation significantly decreased agonist-stimulated cAMP signaling and the number of functional A_{2A}AR molecules on the cell surface.[61] This suggests interactions of cholesterol near position W129 may be more important for maintaining the structural integrity of the receptor rather than signaling. This interpretation is consistent with receptor engineering efforts that introduced tryptophan at the same position in other class A GPCRs when it was not present endogenously to improve receptor expression, stability, and facilitate crystallization.[76,78–83] The results from Figure 5 also suggest cholesterol may play different roles at different interaction sites: cholesterol interaction at W129 may be more important to facilitate receptor stability whereas interactions near R291 may be more involved directly in modulating signaling. The approach described here provides a means for systematically evaluating the potentially different roles of cholesterol at distinct receptor locations.

STAR Methods

RESOURCE AVAILABILITY

Lead Contact—Lead Contact: Dr. Matthew Eddy (matthew.eddy@chem.ufl.edu). Further information and requests for resources or reagents should be directed to and will be fulfilled by the Lead Contact.

Materials Availability—All unique reagents generated in this study are available from the Lead Contact by request and with a completed Materials Transfer Agreement.

Data and Code Availability

- All data reported in this paper will be shared by the lead contact upon request.
- This paper does not report original code.
- Any additional information required to reanalyze the data reported in this paper is available from the lead contact upon request.

EXPERIMENTAL MODEL AND SUBJECT DETAILS

Microbes—XL-10 *E. coli* cells were cultured in LB media, BL21(DE3) and BL21(DE3)-RIL cells were cultured in TB media, and the BG12 strain of *P. pastoris* was cultured in BMGY and BMMY media.

Cell lines—All cell lines used in this study were authenticated by the suppliers and were chosen to remain consistent with previous studies.

METHOD DETAILS

Construct Design—The gene encoding human A_{2A}AR (1-316) was cloned into a pPIC9K vector (Invitrogen) at the BamHI and NotI restriction sites and is consistent with a previously characterized construct.[84 64,85] The gene contained a single amino acid replacement, N154Q, to remove the only glycosylation site in the receptor, an N-terminal FLAG tag, a 10 X C-terminal His tag, and amino acid replacement in helix VII, A289$^{7.54}$C, to generate A_{2A}AR[A289C]. This plasmid was used as a template to perform PCR-based site-directed mutagenesis using the Accuprime Pfx SuperMix (ThermoFisher Scientific) to generate the A_{2A}AR variants R291$^{7.56}$Q, and W129$^{4.50}$I.

A_{2A}AR Production—Plasmids were transformed into competent cells of the *Pichia pastoris* BG12 strain (Biogrammatics). Selection of high-expressing clones was carried out following previously reported protocols,[85] and glycerol stocks of highly expressing clones were prepared and stored for future use.

A_{2A}AR[A289C] and A_{2A}AR[A289C,R291Q] were expressed using the protocol described by Thakur *et al.*.[85] Glycerol stocks of highly expressing colonies were used to inoculate 4 mL cultures in buffered minimal glycerol (BMGY) media, grown at 30 °C for 48 h and used to inoculate 50 mL BMGY medium and grown at 30 °C for 60 h. Each 50 mL culture was used to inoculate 500 mL BMGY medium and grown at 30 °C for 48 h. The

cells were then harvested by centrifugation and then resuspended in 500 mL of buffered minimal methanol (BMMY) media without methanol. Cultures were starved for 6 h at 28 °C to remove remaining glycerol before induction of protein expression by methanol to a final concentration of 0.5% w/v. Two further aliquots of 0.5% w/v methanol were added to the cultures at 12 h intervals after induction for a total expression time of 36 h. A_{2A}AR[A289C,W129I] was expressed with modified conditions; specifically, expression was induced by the addition of methanol to a final concentration of 0.5% w/v at 20 °C in the presence of 1% (v/v) DMSO and 1 mM theophylline. Four further aliquots of 0.5% w/v methanol were added to the cell cultures at 12 h intervals after induction for a total expression time of 64 h. All cells were harvested by centrifugation after the end of the expression period and stored at −80 °C for purification.

A_{2A}AR Purification and ^{19}F-Labeling—Purification and ^{19}F-labeling of A_{2A}AR[A289C] and all A_{2A}AR variants were carried out as described previously.[85 86] Cells expressing A_{2A}AR were resuspended in lysis buffer (50 mM sodium phosphate pH 7.0, 100 mM NaCl, 5% glycerol (w/v), and in-house prepared protease inhibitor solution) and lysed using a cell disruptor (Pressure Biosciences) at 40k PSI. The membranes were isolated by ultracentrifugation at 200,000 * g, homogenized in buffer (10 mM HEPES pH 7.0, 1 M NaCl, 10 mM KCl, and 20 mM $MgCl_2$) and incubated for 1 h at 4 °C with 1 mM of 4,4'-dithiodipyridine (aldrithiol-4) and protease inhibitor cocktail solution (prepared in-house). The suspended membranes were pelleted using ultracentrifugation, homogenized in the same buffer without aldrithiol-4 and incubated with 1 mM of 2,2,2-trifluoroethaethiol (TET) for 1 h at 4°C. The suspended membranes were pelleted again using ultracentrifugation to remove excess TET. The resulting pellet was homogenized in the same buffer without TET and incubated with 1 mM theophylline and protease inhibitor solution for 30 min at 4 °C. Subsequently, protein was extracted from the membrane in a solubilization buffer (50 mM HEPES pH 7.0, 500 mM NaCl, 0.5% (w/v) n-Dodecyl-β-D-Maltopyranoside (DDM), and 0.05% cholesteryl hemisuccinate (CHS)) for 6 hours at 4 °C. Then insolubilized material was separated by ultracentrifugation at 200,000 × g for 30 min, and the supernatant was incubated overnight with Co^{2+}-charged affinity resin (Talon) and 30 mM imidazole at 4 °C. The resin was collected and washed with 20 CV of wash buffer 1 (50 mM HEPES pH 7.0, 500 mM NaCl, 10 mM $MgCl_2$, 30 mM imidazole, 8 mM ATP, 0.05% DDM, and 0.005% CHS), and 20 CV of wash buffer 2 (25 mM HEPES pH 7.0, 250 mM NaCl, 5% glycerol, 30 mM imidazole, 0.05% DDM, 0.005% CHS, and ligand) twice. A_{2A}AR was eluted with an elution buffer (50 mM HEPES pH 7.0, 250 mM NaCl, 5% glycerol, 300 mM imidazole, 0.05% DDM, 0.005% CHS, and ligand) and the protein was finally exchanged into a final buffer (25 mM HEPES pH 7.0, 75 mM NaCl, 0.05% DDM, 0.005% CHS, and ligand), using a PD-10 desalting column (Cytiva) for use in all further experiments. All buffers were prepared with a saturating concentration of the required ligand.

Expression and Purification of MSP1D1—MSP1D1 was expressed and purified following previously described protocols.[85 87] A single colony of BL21(DE3) cells transformed with the MSP1D1 plasmid was used to inoculate 5 mL of LB broth (supplemented with 50 μg/mL of kanamycin) and grown at 37 °C overnight. These 5 mL cultures were consequently used to inoculate 1 L of terrific broth (TB) media and allowed

to grow at 37 °C till the OD_{600nm} reached 0.6–0.8. At this point, protein expression was induced by addition of 1 mM isopropyl β-D-1thiogalactopyranoside (IPTG) and expression was continued for 4 h at 30 °C. The cells were then harvested, and cell pellets were stored at −80 °C for purification. Cell pellets were thawed and resuspended in lysis buffer (50 mM Tris-HCl, pH 8.0, 500 mM NaCl, 1 mM EDTA, 1% triton X-100, and in-house protease inhibitor solution). The cells were lysed using a cell disruptor (Pressure Biosciences) at 20 kPSI and the cell lysate was spun down at 20000 * *g* for 45 min at 4 °C and the resulting supernatant was incubated with Ni-NTA resin (pre-equilibrated with wash buffer 1 (50 mM Tris-HCl, pH 8.0, 500 mM NaCl, and 1% (w/v) Triton X-100)) for 2 h at 4°C. The resin was then collected and washed with 5 CVs of wash buffer 1, 5 CVs of wash buffer 2 (50 mM Tris-HCl, pH 8.0, 500 mM NaCl, and 50 mM cholate), 5 CVs of wash buffer 3 (50 mM Tris-HCl, pH 8.0, and 500 mM NaCl) and finally 5 CVs of wash buffer 4 (50 mM Tris-HCl, pH 8.0, 500 mM NaCl, and 20 mM imidazole). The MSP1D1 was eluted using an elution buffer (50 mM Tris-HCl, pH 8.0, 500 mM NaCl, and 500 mM imidazole). The eluted MSP1D1 was dialyzed against a dialysis buffer (50 mM Tris-HCl, pH 8.0, 20 mM NaCl, and 0.5 mM EDTA) in dialysis tubing with 10 kDa MWCO. Consequently, MSP1D1 was incubated with TEV protease at a ratio of 1:100 (TEV: MSP1D1) (w/w) overnight at 4 °C. Following this, MSP1D1 was isolated by incubating the mixture with Ni-NTA resin and collecting the flow-through. The MSP1D1 was dialyzed in a storage buffer (20 mM Tris-HCl, pH 8.0, 100 mM NaCl, and 0.5 mM EDTA) for 4 h at 4 °C. The purified MSP1D1 was then concentrated to 1 mM, aliquoted and flash frozen for future use.

Nanodisc Assembly—Lipid stocks of POPC, POPC:POPS (70:30, molar ratio), and POPC:POPG (70:30, molar ratio) in chloroform were co-dried with varying amounts of cholesterol to make a lipid film and then vacuum dried for 16 h. The dried lipid film was resuspended in cholate buffer (25 mM Tris-HCl, pH 8.0, 200 mM sodium cholate and 150 mM NaCl) to a final phospholipid concentration of 100 mM.

Nanodiscs samples containing A_{2A}AR were assembled using an earlier described protocol.[85] 27 μM of purified A_{2A}AR was mixed with purified MSP1D1 and detergent-solubilized lipids in a molar ratio of 1:5:250, respectively. After incubation for 2 h at 4 °C, the mixture was incubated overnight with pre-washed bio-beads at 4 °C. Consequently, the bio-beads were removed, and the resulting mixture was incubated with Ni-NTA resin for 24 h at 4 °C. After incubation, the Ni-NTA resin was washed with 2 CV of a wash buffer (50 mM HEPES, pH 7.0, 150 mM NaCl, and 10 mM imidazole), and A_{2A}AR-containing nanodiscs were eluted with an elution buffer (50 mM HEPES, pH 7.0, 150 mM NaCl, 300 mM imidazole and ligand). Using a PD-10 desalting column, all nanodisc samples were exchanged into a final buffer (25 mM HEPES pH 7.0, 75 mM NaCl, 100 μM TFA and ligand) to use for further experiments. All ligand-containing buffers were prepared with a saturating concentration of ligand. All nanodisc samples were characterized using analytical size exclusion chromatography on an Agilent HPLC equipped with a Sepax Nanofilm SEC-200 column operating at a flow rate of 0.5 mL/min. The observed elution time of the nanodisc samples corresponded to particles with an estimated size of approximately 160 KDa, which is consistent with previously reported studies.[88]

Radioligand Binding Assays—Competition binding assays with nanodiscs containing $A_{2A}AR$ were recorded as previously described.[64,89] ZM241385 and NECA binding affinities (K_D or K_I) were determined using competition binding experiments. Increasing concentrations of cold ligands (ZM241385 and NECA) were incubated with 0.0625 μg of $A_{2A}AR$ in nanodiscs in buffer (25 mM HEPES, pH 7.0, and 75 mM NaCl) with 0.5 nM of [^{3}H]ZM241385 for 60 min at 25 °C. Following termination of binding reactions by filtration through Microbeta filtermat-96 cell harvester, radioactivity was measured with a Microbeta2 microplate scintillation counter.

NMR Experiments—NMR samples containing $A_{2A}AR$ in nanodiscs were concentrated to ~200 μM in 280 μL using a Vivaspin-6 concentrator with a 30,000 MWCO. 20 μL of 99.8% D_2O was added[85] and gently mixed with the sample. ^{19}F NMR and ^{31}P NMR experiments were recorded on a Bruker Avance III HD spectrometer operating at 600 MHz ^{1}H nutation frequency using TopSpin 3.6.2 and equipped with a Bruker 5-mm BBFO probe. ^{19}F-NMR spectra were measured at 280 K for direct comparison to earlier results.[64,84] ^{31}P-NMR experiments were measured at 300 K. Temperatures were calibrated from a standard sample of 4% methanol in D_4-MeOH.

The 1-dimensional ^{19}F data were recorded with a data size of 32k complex points, an acquisition period of 360 ms, 16k scans, 120 μs dwell time, and 0.3 s recycle delay for a total experimental time of about 3 hours per experiment. Each final data set averaged six to eight experiments of 16k scans each for total acquisition times between ~18 to ~24 hours. All ^{31}P NMR experiments were acquired with an acquisition time of 900 ms, 2k scans, and 0.3 s recycle delay for a total experiment time of 42 min per experiment.

Quantification of Cholesterol in Nanodisc Samples—The amount of cholesterol in nanodiscs was quantified using the Amplex® Red Cholesterol Assay Kit (Invitrogen) following the manufacturer's protocol. Nanodiscs containing cholesterol were first incubated with 0.2% (v/v) of Triton X-100 for 10 min and then mixed in a 1:1 (v/v) ratio with 1X reaction buffer (300 μM Amplex® Red reagent, 2 U/mL horseradish peroxidase (HRP), 2 U/mL cholesterol oxidase, 0.2 U/mL cholesterol esterase) and incubated in the dark for 30 min at 37 °C. After incubation, fluorescence was detected in a CLARIOstar (BMG Labtech) plate-reader with an excitation range of 530 – 560 nm and emission at 590 nm. For each measurement, the background fluorescence was subtracted, and the resulting fluorescence readout was used to quantify the amount of cholesterol in each nanodisc sample (Table S1). All values reported are mean ± s.e.m for n≥3 independent experiments.

Fluorescence Thermal Shift Assays—Fluorescent thermal shift experiments were carried out following a protocol adapted from earlier publications.[90,91] 10 μg of nanodisc samples was incubated with 10 μM of N-[4-(7-diethylamino-4-methyl-3-coumarinyl)phenyl]maleimide (CPM; Invitrogen) in buffer (50 mM HEPES pH 7.0, 150 mM NaCl) for 30 min on ice in the dark. Fluorescent thermal shift was measured using a Cary Eclipse spectrofluorometer over a temperature range of 20 °C to 90 °C with a fixed heating rate of 2 °C /min. The excitation and emission wavelength for the CPM dye is 387 nm and 463 nm respectively.

$G\alpha_S$ Expression and Purification—Human $G\alpha_S$ containing an N-terminal 6X polyhistidine tag and an N-terminal TEV cleavage site was expressed and purified following a protocol adapted from earlier publications.[92] Glycerol stocks of BL21(DE3)-RIL cells transformed with the $G\alpha_S$ plasmid was were grown in 4 mL LB media (supplemented with 0.2% glucose, 34 μg/mL chloramphenicol and 100 μg/mL carbenicillin) at 37 °C for 8 h. This culture was used to inoculate 75 mL of the same media and continued to grow at 30 °C overnight. After ~16 hours, the cells were harvested and used to inoculate 1 L of M9 media and grown at 30 °C. Protein expression was induced with 50 μM of IPTG when the OD_{600nm} reached 0.8, and expression continued for 16 h at 25 °C. The cells were harvested by centrifugation and stored for future use.

Cells containing $G\alpha_S$ were resuspended in lysis buffer (25 mM Tris-HCl, pH 8.0, 150 mM NaCl, 1 mM $MgCl_2$, 5 μM GDP, in-house protease inhibitor cocktail[85]) and lysed using a cell disruptor at 22 kPSI. The cell lysate was centrifuged at 35,000 × g for 35 min at 4 °C. The lysate was then incubated with Ni-NTA resin overnight at 4 °C. After incubation, the resin was washed with 20 CVs of wash buffer (25 mM Tris-HCl pH 8.0, 500 mM NaCl, 1 mM $MgCl_2$, 5 mM imidazole, 5 μM GDP, and 2 mg/mL iodoacetamide) and the protein was eluted using an elution buffer (25 mM Tris-HCl pH 8.0, 250 mM NaCl, 1 mM $MgCl_2$, 250 mM imidazole, 10% (v/v) glycerol, and 5 μM GDP). The eluted protein was exchanged into buffer (25 mM Tris-HCl pH 8.0, 100 mM NaCl, 1 mM $MgCl_2$, 10% (v/v) glycerol, 5 μM GDP) and incubated with TEV protease at a ratio of 1:50 (TEV: $G\alpha_S$) (w/w) overnight at 4 °C. Following this, $G\alpha_S$ was isolated by incubating the mixture with Ni-NTA resin and collecting the flow-through. $G\alpha_S$ was further purified by gel-filtration with buffer (20 mM HEPES pH 8.0, 150 mM NaCl, 5 mM $MgCl_2$, 1 mM EDTA, 10% (v/v) glycerol, and 5 μM GDP), concentrated to 50 μM and either immediately used or frozen and stored for future use.

Membrane Fluidity Measurements—Nanodiscs containing POPC and various amounts of cholesterol were prepared and mixed with Laurdan (Tocris Bioscience) at a molar ratio of 500:1 (total lipids:Laurdan), and the mixture was incubated in the dark at 25 °C for 1 hour. Following this, excess Laurdan was removed *via* buffer exchange using a PD MiniTrap G-25 column (Cytiva) equilibrated with buffer (25 mM HEPES pH 7.0 and 75 mM NaCl). Fluorescence emission curves for Laurdan embedded in nanodiscs were measured in a Cary Eclipse spectrofluorometer, using an excitation wavelength of 366 nm and observing emission between 400 nm and 600 nm.

GTP Hydrolysis Assay—GTP turnover for $A_{2A}AR$ in nanodiscs was measured using the GTPase-Glo™ assay (Promega) following manufacturer's protocols. Purified nanodiscs containing $A_{2A}AR$ were mixed with the $G\alpha_s$ protein in a molar ratio of 4:1 in the presence of 5 μM GTP in buffer (25 mM HEPES pH 7.0, 75 mM NaCl) and incubated for 1 hour. Subsequently, GTP turnover was measured using a luminescence readout on a CLARIOstar (BMG Labtech) plate-reader.

QUANTIFICATION AND STATISTICAL ANALYSIS

Radioligand Binding Data Analysis—All radioligand competition experiments were conducted with 3 or more replicates. IC_{50} values were determined using a nonlinear, least-square regression analysis in Prism 8 (GraphPad Software, Inc.). The K_I values were calculated from the IC_{50} using the Cheng−Prusoff equation.[93] Error bars for each sample were calculated as the standard error of mean (s.e.m) for 3 independent experiments done in triplicate.

Fluorescence Thermal Shift Data Analysis—The raw data were fit according to previously reported procedures[90] and analyzed using Origin (OriginLab Corporation). The raw data was fit to a Boltzmann sigmoidal curve to determine the melting temperature (T_m). The error bars are reported as standard error of mean (s.e.m) for 3 or more independent experiments.

Membrane Fluidity Data Analysis—The emission spectra were normalized to the corresponding emission maxima. Following the protocol from Yu et al.,[71] the generalized polarization (GP) of Laurdan was calculated using the formula:

$$GP = (I_{440} - I_{490})/(I_{440} + I_{490})$$

where I_{440} and I_{490} are the fluorescence emission intensities at 440 nm and 490 nm, respectively. All GP values reported are the mean ± s.e.m. for 3 independent measurements.

GTP Hydrolysis Assay Analysis—The percentage of GTP hydrolyzed was calculated by subtracting background luminescence. All values reported in Table 3 are the mean ± s.e.m. for 3 or more independent experiments. To determine the statistical significance of reported differences in GTP hydrolysis, statistical analysis was conducted using a two-tailed unpaired t-test. P values less than 0.05 were considered to be statistically significant. Statistically significant values are illustrated as *P<0.05, **P<0.005, and ***P<0.0005, respectively.

NMR Data Analysis—All NMR data were processed and analyzed in Topspin 4.0.8 (Bruker Biospin). Prior to Fourier transformation, all 1-dimensional ^{19}F-NMR data were zero-filled to 64k points and multiplied by an exponential window function with 40 Hz line broadening. All ^{19}F spectra were referenced to a TFA signal at −75.8 ppm, which was set to 0 ppm. Deconvolution of the overlapping ^{19}F-NMR data were done in accordance to previously published procedures[64,84] with MestreNova version 14.1.1–24571 (MestreLab Research S.L). The ^{19}F-NMR spectra were fit to double- or triple-Lorentzian functions, and the quality of the fits was assessed from the residual difference of the experimental data and the sum of the computed components. The relative populations of A_{2A}AR conformational states were calculated as a ratio of the integrated area of each deconvoluted peak with respect to the total integral of all signals from 7.5 ppm to 14.5 ppm.

All ^{31}P NMR data were processed identically. Prior to Fourier transformation, ^{31}P spectra were zero-filled to 64k points and multiplied by an exponential window function with 50 Hz line broadening.

Supplementary Material

Refer to Web version on PubMed Central for supplementary material.

ACKNOWLEDGEMENTS

This work is supported by the National Institutes of Health, NIGMS MIRA grant R35GM138291 (M.T.E., N.T., A.R. and N.G.P). A portion of this work was supported by the McKnight Brain Institute at the National High Magnetic Field Laboratory's AMRIS Facility, which is funded by National Science Foundation Cooperative Agreement No. DMR-1644779 and the State of Florida

References:

1. Yeagle PL (2014). Non-covalent binding of membrane lipids to membrane proteins. Biochimica et Biophysica Acta (BBA) - Biomembranes 1838, 1548–1559. 10.1016/J.BBAMEM.2013.11.009. [PubMed: 24269542]
2. Yeagle PL (1991). Modulation of membrane function by cholesterol. Biochimie 73, 1303–1310. 10.1016/0300-9084(91)90093-G. [PubMed: 1664240]
3. Elkins MR, Williams JK, Gelenter MD, Dai P, Kwon B, Sergeyev IV, Pentelute BL, and Hong M (2017). Cholesterol-binding site of the influenza M2 protein in lipid bilayers from solid-state NMR. Proc. Natl. Acad. Sci 114, 12946–12951. 10.1073/pnas.1715127114. [PubMed: 29158386]
4. Fantini J, and Barrantes FJ (2013). How cholesterol interacts with membrane proteins: an exploration of cholesterol-binding sites including CRAC, CARC, and tilted domains. Front. Physiol 4. 10.3389/fphys.2013.00031.
5. Epand RM (2006). Cholesterol and the interaction of proteins with membrane domains. Prog. Lipid Res 45, 279–294. 10.1016/j.plipres.2006.02.001. [PubMed: 16574236]
6. Grouleff J, Irudayam SJ, Skeby KK, and Schiøtt B (2015). The influence of cholesterol on membrane protein structure, function, and dynamics studied by molecular dynamics simulations. Biochimica et Biophysica Acta (BBA) - Biomembranes 1848, 1783–1795. 10.1016/J.BBAMEM.2015.03.029. [PubMed: 25839353]
7. Carruthers A, and Melchior DL (1986). How bilayer lipids affect membrane protein activity. Trends Biochem. Sci 11, 331–335. 10.1016/0968-0004(86)90292-6.
8. Song Y, Kenworthy AK, and Sanders CR (2014). Cholesterol as a co-solvent and a ligand for membrane proteins: Cholesterol-Protein Interactions. Protein Sci. 23, 1–22. 10.1002/pro.2385.
9. Bastiaanse E (1997). The effect of membrane cholesterol content on ion transport processes in plasma membranes. Cardiovasc. Res 33, 272–283. 10.1016/S0008-6363(96)00193-9. [PubMed: 9074689]
10. Di Paolo G, and Kim T-W (2011). Linking lipids to Alzheimer's disease: cholesterol and beyond. Nat. Rev. Neurosci 12, 284–296. 10.1038/nrn3012. [PubMed: 21448224]
11. Goldstein Joseph L., and Brown Michael S. (2015). A Century of Cholesterol and Coronaries: From Plaques to Genes to Statins. Cell 161, 161–172. 10.1016/j.cell.2015.01.036. [PubMed: 25815993]
12. Perego C, Da Dalt L, Pirillo A, Galli A, Catapano AL, and Norata GD (2019). Cholesterol metabolism, pancreatic β-cell function and diabetes. Biochim. Biophys. Acta Mol. Basis Dis 1865, 2149–2156. 10.1016/j.bbadis.2019.04.012. [PubMed: 31029825]
13. Hauser AS, Attwood MM, Rask-Andersen M, Schiöth HB, and Gloriam DE (2017). Trends in GPCR drug discovery: new agents, targets and indications. Nat. Rev. Drug Disc 16, 829–842. 10.1038/nrd.2017.178.

14. Duncan AL, Song W, and Sansom MSP (2020). Lipid-Dependent Regulation of Ion Channels and G Protein–Coupled Receptors: Insights from Structures and Simulations. Annual Review of Pharmacology and Toxicology 60, 31–50. 10.1146/ANNUREV-PHARMTOX-010919-023411.
15. Guixà-González R, Albasanz JL, Rodriguez-Espigares I, Pastor M, Sanz F, Martí-Solano M, Manna M, Martinez-Seara H, Hildebrand PW, Martín M, and Selent J (2017). Membrane cholesterol access into a G-protein-coupled receptor. Nat. Comm 8, 1–12. 10.1038/ncomms14505.
16. Hedger G, Koldsø H, Chavent M, Siebold C, Rohatgi R, and Sansom MSP (2019). Cholesterol Interaction Sites on the Transmembrane Domain of the Hedgehog Signal Transducer and Class F G Protein-Coupled Receptor Smoothened. Structure 27, 549–559.e542. 10.1016/j.str.2018.11.003. [PubMed: 30595453]
17. Deshpande I, Liang J, Hedeen D, Roberts KJ, Zhang Y, Ha B, Latorraca NR, Faust B, Dror RO, Beachy PA, et al. (2019). Smoothened stimulation by membrane sterols drives Hedgehog pathway activity. Nature 571, 284–288. 10.1038/s41586-019-1355-4. [PubMed: 31263273]
18. Saxena R, and Chattopadhyay A (2012). Membrane cholesterol stabilizes the human serotonin1A receptor. Biochimica et Biophysica Acta (BBA) - Biomembranes 1818, 2936–2942. 10.1016/J.BBAMEM.2012.07.032. [PubMed: 22892071]
19. Lu M, Zhao W, Han S, Lin X, Xu T, Tan Q, Wang M, Yi C, Chu X, Yang W, et al. (2022). Activation of the human chemokine receptor CX3CR1 regulated by cholesterol. Science Advances 8, 8048–8048. 10.1126/SCIADV.ABN8048/SUPPL_FILE/SCIADV.ABN8048_SM.PDF.
20. Gimpl G, Klein U, Reilaender H, and Fahrenholz F (1995). Expression of the Human Oxytocin Receptor in Baculovirus-Infected Insect Cells: High-Affinity Binding Is Induced by a Cholesterol-Cyclodextrin Complex. Biochemistry 34, 13794–13801. 10.1021/bi00042a010. [PubMed: 7577972]
21. Babcock GJ, Farzan M, and Sodroski J (2003). Ligand-independent Dimerization of CXCR4, a Principal HIV-1 Coreceptor. J. Biol. Chem 278, 3378–3385. 10.1074/jbc.M210140200. [PubMed: 12433920]
22. Chattopadhyay A, Jafurulla M, Kalipatnapu S, Pucadyil TJ, and Harikumar KG (2005). Role of cholesterol in ligand binding and G-protein coupling of serotonin1A receptors solubilized from bovine hippocampus. Biochem. Biophys. Res. Commun 327, 1036–1041. 10.1016/j.bbrc.2004.12.102. [PubMed: 15652500]
23. Ruthirakuhan M, Herrmann N, Andreazza AC, Verhoeff NPLG, Gallagher D, Black SE, Kiss A, and Lanctôt KL (2019). 24S-Hydroxycholesterol Is Associated with Agitation Severity in Patients with Moderate-to-Severe Alzheimer's Disease: Analyses from a Clinical Trial with Nabilone. J. Alzheimers Dis 71, 21–31. 10.3233/JAD-190202. [PubMed: 31322567]
24. Calmet P, Cullin C, Cortès S, Vang M, Caudy N, Baccouch R, Dessolin J, Maamar NT, Lecomte S, Tillier B, and Alves ID (2020). Cholesterol impacts chemokine CCR5 receptor ligand-binding activity. FEBS J. 287, 2367–2385. 10.1111/febs.15145. [PubMed: 31738467]
25. Luchetti G, Sircar R, Kong JH, Nachtergaele S, Sagner A, Byrne EF, Covey DF, Siebold C, and Rohatgi R (2016). Cholesterol activates the G-protein coupled receptor Smoothened to promote Hedgehog signaling. eLife 5, e20304. 10.7554/eLife.20304. [PubMed: 27705744]
26. Pluhackova K, Gahbauer S, Kranz F, Wassenaar TA, and Böckmann RA (2016). Dynamic Cholesterol-Conditioned Dimerization of the G Protein Coupled Chemokine Receptor Type 4. PLoS Comput. Biol. 12, e1005169. 10.1371/journal.pcbi.1005169.
27. Sengupta D, Kumar GA, and Chattopadhyay A (2017). Interaction of Membrane Cholesterol with GPCRs: Implications in Receptor Oligomerization. In G-Protein-Coupled Receptor Dimers, Herrick-Davis K, Milligan G, and Di Giovanni G, eds. (Springer International Publishing), pp. 415–429.
28. Prasanna X, Sengupta D, and Chattopadhyay A (2016). Cholesterol-dependent Conformational Plasticity in GPCR Dimers. Sci. Rep 6, 31858. 10.1038/srep31858. [PubMed: 27535203]
29. Chakraborty H, and Chattopadhyay A (2015). Excitements and Challenges in GPCR Oligomerization: Molecular Insight from FRET. ACS Chem. Neurosci 6, 199–206. 10.1021/cn500231d. [PubMed: 25363209]

30. Kumar GA, Sarkar P, Stepniewski TM, Jafurulla M, Singh SP, Selent J, and Chattopadhyay A (2021). A molecular sensor for cholesterol in the human serotonin $_{1A}$ receptor. Sci. Adv 7, eabh2922. 10.1126/sciadv.abh2922. [PubMed: 34301606]
31. Kumar GA, and Chattopadhyay A (2020). Statin-Induced Chronic Cholesterol Depletion Switches GPCR Endocytosis and Trafficking: Insights from the Serotonin $_{1A}$ Receptor. ACS Chem. Neurosci 11, 453–465. 10.1021/acschemneuro.9b00659. [PubMed: 31880914]
32. Maza N, Wang D, Kowalski C, Stoveken HM, Dao M, Sial OK, Giles AC, Grill B, and Martemyanov KA (2022). Ptchd1 mediates opioid tolerance via cholesterol-dependent effects on μ-opioid receptor trafficking. Nat. Neurosci 25, 1179–1190. 10.1038/s41593-022-01135-0. [PubMed: 35982154]
33. Kunselman JM, Lott J, and Puthenveedu MA (2021). Mechanisms of selective G protein–coupled receptor localization and trafficking. Curr. Opin. Cell Biol 71, 158–165. 10.1016/j.ceb.2021.03.002. [PubMed: 33965654]
34. Yeliseev A, Iyer MR, Joseph TT, Coffey NJ, Cinar R, Zoubak L, Kunos G, and Gawrisch K (2021). Cholesterol as a modulator of cannabinoid receptor CB2 signaling. Sci. Rep 11, 3706. 10.1038/s41598-021-83245-6. [PubMed: 33580091]
35. Meyerowitz JG, Robertson MJ, Barros-Álvarez X, Panova O, Nwokonko RM, Gao Y, and Skiniotis G (2022). The oxytocin signaling complex reveals a molecular switch for cation dependence. Nat. Struct. Mol. Biol 29, 274–281. 10.1038/s41594-022-00728-4. [PubMed: 35241813]
36. Oates J, and Watts A (2011). Uncovering the intimate relationship between lipids, cholesterol and GPCR activation. Curr. Opin. Struct. Biol 21, 802–807. 10.1016/j.sbi.2011.09.007. [PubMed: 22036833]
37. Sarkar P, and Chattopadhyay A (2020). Cholesterol interaction motifs in G protein-coupled receptors: Slippery hot spots? WIREs Syst. Biol. Med 12. 10.1002/wsbm.1481.
38. Gater Deborah L., Saurel O, Iordanov I, Liu W, Cherezov V, and Milon A (2014). Two Classes of Cholesterol Binding Sites for the β 2 AR Revealed by Thermostability and NMR. Biophys. J 107, 2305–2312. 10.1016/j.bpj.2014.10.011. [PubMed: 25418299]
39. Abiko LA, Dias Teixeira R, Engilberge S, Grahl A, Mühlethaler T, Sharpe T, and Grzesiek S (2022). Filling of a water-free void explains the allosteric regulation of the β1-adrenergic receptor by cholesterol. Nat. Chem 14, 1133–1141. 10.1038/s41557-022-01009-9. [PubMed: 35953642]
40. Albert AD, Young JE, and Yeagle PL (1996). Rhodopsin-cholesterol interactions in bovine rod outer segment disk membranes. Biochim. Biophys. Acta Biomembr 1285, 47–55. 10.1016/S0005-2736(96)00145-9.
41. Mitchell DC, Straume M, Miller JL, and Litman BJ (1990). Modulation of metarhodopsin formation by cholesterol-induced ordering of bilayer lipids. Biochemistry 29, 9143–9149. 10.1021/bi00491a007. [PubMed: 2271584]
42. Lebon G, Warne T, Edwards PC, Bennett K, Langmead CJ, Leslie AGW, and Tate CG (2011). Agonist-bound adenosine A2A receptor structures reveal common features of GPCR activation. Nature 2011 474:7352 474, 521–525. 10.1038/nature10136.
43. García-Nafría J, Lee Y, Bai X, Carpenter B, and Tate CG (2018). Cryo-EM structure of the adenosine A2A receptor coupled to an engineered heterotrimeric G protein. eLife 7. 10.7554/eLife.35946.001.
44. Carpenter B, Nehmé R, Warne T, Leslie AGW, and Tate CG (2016). Structure of the adenosine A2A receptor bound to an engineered G protein. Nature 536, 104–107. 10.1038/nature18966. [PubMed: 27462812]
45. Liu W, Chun E, Thompson AA, Chubukov P, Xu F, Katritch V, Han GW, Roth CB, Heitman LH, IJzerman AP, et al. (2012). Structural Basis for Allosteric Regulation of GPCRs by Sodium Ions. Science 337, 232–236. 10.1126/science.1219218. [PubMed: 22798613]
46. Jaakola V-P, Griffith MT, Hanson MA, Cherezov V, Chien EYT, Lane JR, IJzerman AP, and Stevens RC (2008). The 2.6 angstrom crystal structure of a human A_{2A} adenosine receptor bound to an antagonist. Science 322, 1211–1217. 10.1126/science.1164772. [PubMed: 18832607]
47. Huang SK, Pandey A, Tran DP, Villanueva NL, Kitao A, Sunahara RK, Sljoka A, and Prosser RS (2021). Delineating the conformational landscape of the adenosine A2A receptor during G protein coupling. Cell 184, 1884–1894. 10.1016/j.cell.2021.02.041. [PubMed: 33743210]

48. Ye L, Van Eps N, Zimmer M, Ernst OP, and Scott Prosser R (2016). Activation of the A2A adenosine G-protein-coupled receptor by conformational selection. Nature 533, 265–268. 10.1038/nature17668. [PubMed: 27144352]
49. Eddy MT, Martin BT, and Wüthrich K (2021). A2A adenosine receptor partial agonism related to structural rearrangements in an activation microswitch. Structure 29, 170–176. 10.1016/j.str.2020.11.005. [PubMed: 33238145]
50. Eddy MT, Lee M-Y, Gao Z-G, White KL, Didenko T, Horst R, Audet M, Stanczak P, McClary KM, Han GW, et al. (2018). Allosteric coupling of drug binding and intracellular signaling in the A2A adenosine receptor. Cell 172, 68–80. 10.1016/j.cell.2017.12.004. [PubMed: 29290469]
51. Sušac L, Eddy MT, Didenko T, Stevens RC, and Wüthrich K (2018). A2A adenosine receptor functional states characterized by 19F-NMR. Proc. Natl. Acad. Sci 115, 12733–12738. 10.1073/pnas.1813649115. [PubMed: 30463958]
52. Eddy MT, Gao Z-G, Mannes P, Patel N, Jacobson KA, Katritch V, Stevens RC, and Wüthrich K (2018). Extrinsic tryptophans as NMR probes of allosteric coupling in membrane proteins: application to the A_{2A} adenosine receptor. J. Am. Chem. Soc 140, 8228–8235. 10.1021/jacs.8b03805. [PubMed: 29874058]
53. Mizumura T, Kondo K, Kurita M, Kofuku Y, Natsume M, Imai S, Shiraishi Y, Ueda T, and Shimada I (2020). Activation of adenosine A_{2A} receptor by lipids from docosahexaenoic acid revealed by NMR. Science Advances 6, eaay8544. 10.1126/sciadv.aay8544. [PubMed: 32206717]
54. Bara-Jimenez W, Sherzai A, Dimitrova T, Favit A, Bibbiani F, Gillespie M, Morris MJ, Mouradian MM, and Chase TN (2003). Adenosine A2A receptor antagonist treatment of Parkinson's disease. Neurology 61, 293–296. 10.1212/01.WNL.0000073136.00548.D4. [PubMed: 12913186]
55. Young A, Ngiow SF, Barkauskas DS, Sult E, Hay C, Blake SJ, Huang Q, Liu J, Takeda K, Teng MWL, et al. (2016). Co-inhibition of CD73 and A2AR Adenosine Signaling Improves Anti-tumor Immune Responses. Cancer Cell 30, 391–403. 10.1016/J.CCELL.2016.06.025. [PubMed: 27622332]
56. McGraw C, Yang L, Levental I, Lyman E, and Robinson AS (2019). Membrane cholesterol depletion reduces downstream signaling activity of the adenosine A2A receptor. Biochim. Biophys. Acta Biomembr 1861, 760–767. 10.1016/j.bbamem.2019.01.001. [PubMed: 30629951]
57. Rouviere E, Arnarez C, Yang L, and Lyman E (2017). Identification of Two New Cholesterol Interaction Sites on the A2A Adenosine Receptor. Biophys. J 113, 2415–2424. 10.1016/j.bpj.2017.09.027. [PubMed: 29211995]
58. Song W, Yen HY, Robinson CV, and Sansom MSP (2019). State-dependent Lipid Interactions with the A2a Receptor Revealed by MD Simulations Using In Vivo-Mimetic Membranes. Structure 27, 392–403.e393. 10.1016/j.str.2018.10.024. [PubMed: 30581046]
59. Lovera S, Cuzzolin A, Kelm S, De Fabritiis G, and Sands ZA (2019). Reconstruction of apo A2A receptor activation pathways reveal ligand-competent intermediates and state-dependent cholesterol hotspots. Sci. Rep 9, 14199. 10.1038/s41598-019-50752-6. [PubMed: 31578448]
60. Huang SK, Almurad O, Pejana RJ, Morrison ZA, Pandey A, Picard L-P, Nitz M, Sljoka A, and Prosser RS (2022). Allosteric modulation of the adenosine A2A receptor by cholesterol. eLife 11, e73901. 10.7554/eLife.73901. [PubMed: 34986091]
61. McGraw C, Koretz KS, Oseid D, Lyman E, and Robinson AS (2022). Cholesterol Dependent Activity of the Adenosine A2A Receptor Is Modulated via the Cholesterol Consensus Motif. Molecules 27, 3529. [PubMed: 35684466]
62. Taghon GJ, Rowe JB, Kapolka NJ, and Isom DG (2021). Predictable cholesterol binding sites in GPCRs lack consensus motifs. Structure 29, 499–506.e493. 10.1016/j.str.2021.01.004. [PubMed: 33508215]
63. Song W, Yen H-Y, Robinson CV, and Sansom MSP (2019). State-dependent lipid interactions with the A2a receptor revealed by MD simulations using in vivo-mimetic membranes. Structure 27, 392–403. 10.1016/j.str.2018.10.024. [PubMed: 30581046]
64. Thakur N, Ray AP, Sharp L, Jin B, Duong A, Pour NG, Obeng S, Wijesekara AV, Gao Z-G, McCurdy CR, et al. (2023). Anionic phospholipids control mechanisms of GPCR-G protein recognition. Nat. Comm 14, 794. 10.1038/s41467-023-36425-z.

65. van Aalst E, and Wylie BJ (2021). Cholesterol Is a Dose-Dependent Positive Allosteric Modulator of CCR3 Ligand Affinity and G Protein Coupling. Front. Mol. Biosci 8. 10.3389/fmolb.2021.724603.
66. Scheidelaar S, Koorengevel Martijn C., Pardo Juan D., Meeldijk Johannes D., Breukink E, and Killian JA (2015). Molecular Model for the Solubilization of Membranes into Nanodisks by Styrene Maleic Acid Copolymers. Biophys. J 108, 279–290. 10.1016/j.bpj.2014.11.3464. [PubMed: 25606677]
67. Harayama T, and Riezman H (2018). Understanding the diversity of membrane lipid composition. Nat. Rev. Mol. Cell Biol 19, 281–296. 10.1038/nrm.2017.138. [PubMed: 29410529]
68. Amundson DM, and Zhou M (1999). Fluorometric method for the enzymatic determination of cholesterol. Journal of Biochemical and Biophysical Methods 38, 43–52. 10.1016/S0165-022X(98)00036-0. [PubMed: 10078872]
69. Oliveira FFM, Paes HC, Peconick LDF, Fonseca FL, Marina CLF, Bocca AL, Homem-de-Mello M, Rodrigues ML, Albuquerque P, Nicola AM, et al. (2020). Erg6 affects membrane composition and virulence of the human fungal pathogen Cryptococcus neoformans. Fungal Genet. Biol 140, 103368. 10.1016/j.fgb.2020.103368. [PubMed: 32201128]
70. Sušac L, O'Connor C, Stevens RC, and Wüthrich K (2015). In-membrane chemical modification (IMCM) for site-specific chromophore labeling of GPCRs. Angew. Chem 127, 15461–15464. 10.1002/ange.201508506.
71. Yu W, So PT, French T, and Gratton E (1996). Fluorescence generalized polarization of cell membranes: a two-photon scanning microscopy approach. Biophys. J 70, 626–636. 10.1016/S0006-3495(96)79646-7. [PubMed: 8789081]
72. Jakubík J, and El-Fakahany EE (2021). Allosteric Modulation of GPCRs of Class A by Cholesterol. Int. J. Mol. Sci 22, 1953–1953. 10.3390/IJMS22041953. [PubMed: 33669406]
73. Mondal S, Hsiao K, and Goueli SA (2015). A Homogenous Bioluminescent System for Measuring GTPase, GTPase Activating Protein, and Guanine Nucleotide Exchange Factor Activities. ASSAY and Drug Development Technologies 13, 444–455. 10.1089/adt.2015.643. [PubMed: 26167953]
74. Lee JY, Patel R, and Lyman E (2013). Ligand-dependent cholesterol interactions with the human A2A adenosine receptor. Chemistry and Physics of Lipids 169, 39–45. 10.1016/j.chemphyslip.2013.02.002. [PubMed: 23454349]
75. Ballesteros JA, and Weinstein H (1995). Integrated methods for the construction of three-dimensional models and computational probing of structure-function relations in G protein-coupled receptors. In Methods in neurosciences, (Elsevier), pp. 366–428.
76. Hanson MA, Cherezov V, Griffith MT, Roth CB, Jaakola V-P, Chien EYT, Velasquez J, Kuhn P, and Stevens RC (2008). A Specific Cholesterol Binding Site Is Established by the 2.8 Å Structure of the Human β2-Adrenergic Receptor. Structure 16, 897–905. 10.1016/j.str.2008.05.001. [PubMed: 18547522]
77. Denisov IG, and Sligar SG (2017). Nanodiscs in Membrane Biochemistry and Biophysics. Chem. Rev 117, 4669–4713. 10.1021/acs.chemrev.6b00690. [PubMed: 28177242]
78. Roth CB, Hanson MA, and Stevens RC (2008). Stabilization of the Human β2-Adrenergic Receptor TM4–TM3–TM5 Helix Interface by Mutagenesis of Glu1223.41, A Critical Residue in GPCR Structure. J. Mol. Biol 376, 1305–1319. 10.1016/j.jmb.2007.12.028. [PubMed: 18222471]
79. Cherezov V, Rosenbaum DM, Hanson MA, Rasmussen SGF, Thian FS, Kobilka TS, Choi H-J, Kuhn P, Weis WI, Kobilka BK, and Stevens RC (2007). High-Resolution Crystal Structure of an Engineered Human β_2-Adrenergic G Protein–Coupled Receptor. Science 318, 1258–1265. 10.1126/science.1150577. [PubMed: 17962520]
80. Johansson LC, Stauch B, McCorvy JD, Han GW, Patel N, Huang X-P, Batyuk A, Gati C, Slocum ST, Li C, et al. (2019). XFEL structures of the human MT2 melatonin receptor reveal the basis of subtype selectivity. Nature 569, 289–292. 10.1038/s41586-019-1144-0. [PubMed: 31019305]
81. Stauch B, Johansson LC, McCorvy JD, Patel N, Han GW, Huang X-P, Gati C, Batyuk A, Slocum ST, Ishchenko A, et al. (2019). Structural basis of ligand recognition at the human MT1 melatonin receptor. Nature 569, 284–288. 10.1038/s41586-019-1141-3. [PubMed: 31019306]

82. Wacker D, Wang C, Katritch V, Han GW, Huang X-P, Vardy E, McCorvy JD, Jiang Y, Chu M, Siu FY, et al. (2013). Structural Features for Functional Selectivity at Serotonin Receptors. Science 340, 615–619. 10.1126/science.1232808. [PubMed: 23519215]
83. Chien EYT, Liu W, Zhao Q, Katritch V, Won Han G, Hanson MA, Shi L, Newman AH, Javitch JA, Cherezov V, and Stevens RC (2010). Structure of the Human Dopamine D3 Receptor in Complex with a D2/D3 Selective Antagonist. Science 330, 1091–1095. 10.1126/science.1197410. [PubMed: 21097933]
84. Sušac L, Eddy MT, Didenko T, Stevens RC, and Wüthrich K (2018). A2A adenosine receptor functional states characterized by 19F-NMR. Proceedings of the National Academy of Sciences of the United States of America 115, 12733–12738. 10.1073/pnas.1813649115. [PubMed: 30463958]
85. Thakur N, Wei S, Ray AP, Lamichhane R, and Eddy MT (2022). Production of human A2AAR in lipid nanodiscs for 19F-NMR and single-molecule fluorescence spectroscopy. STAR Protocols 3, 101535–101535. 10.1016/J.XPRO.2022.101535. [PubMed: 35839771]
86. Sušac L, O'Connor C, Stevens RC, and Wüthrich K (2015). In-Membrane Chemical Modification (IMCM) for Site-Specific Chromophore Labeling of GPCRs. Angew Chem Int Ed Engl 54, 15246–15249. 10.1002/anie.201508506. [PubMed: 26545333]
87. Hagn F, Nasr ML, and Wagner G (2018). Assembly of phospholipid nanodiscs of controlled size for structural studies of membrane proteins by NMR. Nat Protoc 13, 79–98. 10.1038/nprot.2017.094. [PubMed: 29215632]
88. Thakur N, Wei S, Ray AP, Lamichhane R, and Eddy MT (2022). Production of human A2AAR in lipid nanodiscs for 19F-NMR and single-molecule fluorescence spectroscopy. STAR Protocols 3, 101535. 10.1016/j.xpro.2022.101535. [PubMed: 35839771]
89. Wei S, Thakur N, Ray AP, Jin B, Obeng S, McCurdy CR, McMahon LR, Gutiérrez-de-Terán H, Eddy MT, and Lamichhane R (2022). Slow conformational dynamics of the human A2A adenosine receptor are temporally ordered. Structure 30, 329–337.e325. 10.1016/J.STR.2021.11.005. [PubMed: 34895472]
90. Alexandrov AI, Mileni M, Chien EYT, Hanson MA, and Stevens RC (2008). Microscale Fluorescent Thermal Stability Assay for Membrane Proteins. Structure 16, 351–359. 10.1016/j.str.2008.02.004. [PubMed: 18334210]
91. White KL, Eddy MT, Gao ZG, Han GW, Lian T, Deary A, Patel N, Jacobson KA, Katritch V, and Stevens RC (2018). Structural Connection between Activation Microswitch and Allosteric Sodium Site in GPCR Signaling. Structure 26, 259–269.e255. 10.1016/j.str.2017.12.013. [PubMed: 29395784]
92. Hu Q, and Shokat KM (2018). Disease-causing mutations in the G protein Gαs subvert the roles of GDP and GTP. Cell 173, 1254–1264. e1211. [PubMed: 29628140]
93. Cheng Y, and Prusoff WH (1973). Relationship between the inhibition constant (K1) and the concentration of inhibitor which causes 50 per cent inhibition (I50) of an enzymatic reaction. Biochem. Pharmacol 22, 3099–3108. 10.1016/0006-2952(73)90196-2. [PubMed: 4202581]

Highlights

- Specific cholesterol-A_{2A}AR interactions activate receptor in POPC lipid bilayers
- Influence of sterols on agonist-bound A_{2A}AR observed with cholesterol analogs
- Cholesterol and anionic lipids share complementary roles in A_{2A}AR activation
- Different cholesterol interaction sites distinctly impact structure and function

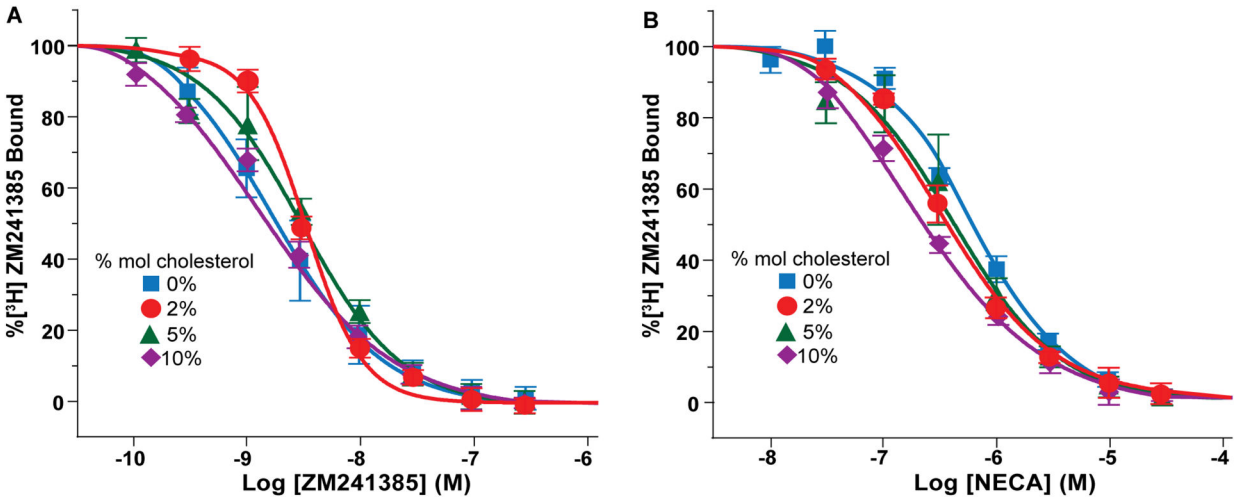

Figure 1. Pharmacological activity of A_{2A}AR[A289C] in lipid nanodiscs containing varying amounts of cholesterol.

(A) Homologous competition binding experiments with the antagonist ZM241385. Data were measured for A_{2A}AR[A289C] prepared in nanodiscs containing POPC and varying amounts of cholesterol, as indicated. Error bars indicate the s.e.m for 3 independent trials done in triplicate. The determined K_D values are listed in Table S2.

(B) Competition binding experiments with the agonist NECA for A_{2A}AR[A289C] prepared in nanodiscs containing POPC and varying amounts of cholesterol. Same presentation details as (A). The determined K_I values are listed in Table S2. See also Figure S1, Figure S3 and Table S1.

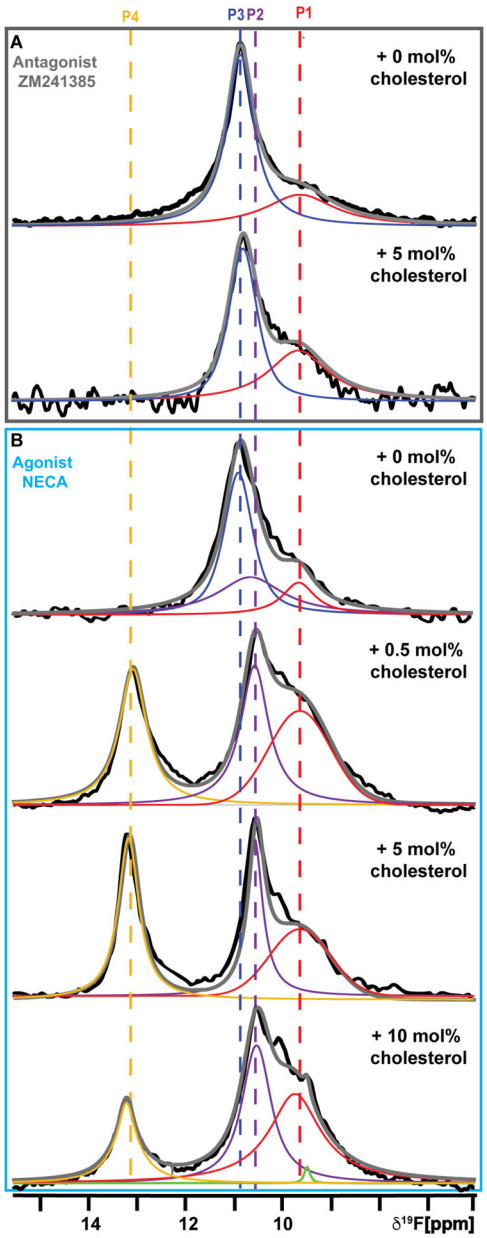

Figure 2. NMR-observed conformational states of $A_{2A}AR[A289C^{TET}]$ in nanodiscs with POPC and varying amounts of cholesterol.

(A) The 1-dimensional ^{19}F-NMR spectra of $A_{2A}AR[A289C^{TET}]$ in complex with the antagonist ZM241385 in nanodiscs containing POPC and without cholesterol or with 5 mol% cholesterol.

(B) The 1-dimensional ^{19}F-NMR spectra of $A_{2A}AR[A289C^{TET}]$ in complex with the agonist NECA in nanodiscs containing POPC and varying amounts of cholesterol, as indicated. The NMR spectra shown are interpreted using Lorentzian deconvolutions with the minimal number of components required to provide a good fit, labeled P1 to P4. The grey lines superimposed on the spectra are the total sums of the individual deconvolutions. The green line superimposed on the bottom spectrum is a Lorentzian deconvolution of a minor contribution from free TET present in this sample. The chemical shifts of P1 to P4 are

indicated by the colored dashed vertical lines. See also Figures S3 – S6, Figure S11, Table S3, and Table S4.

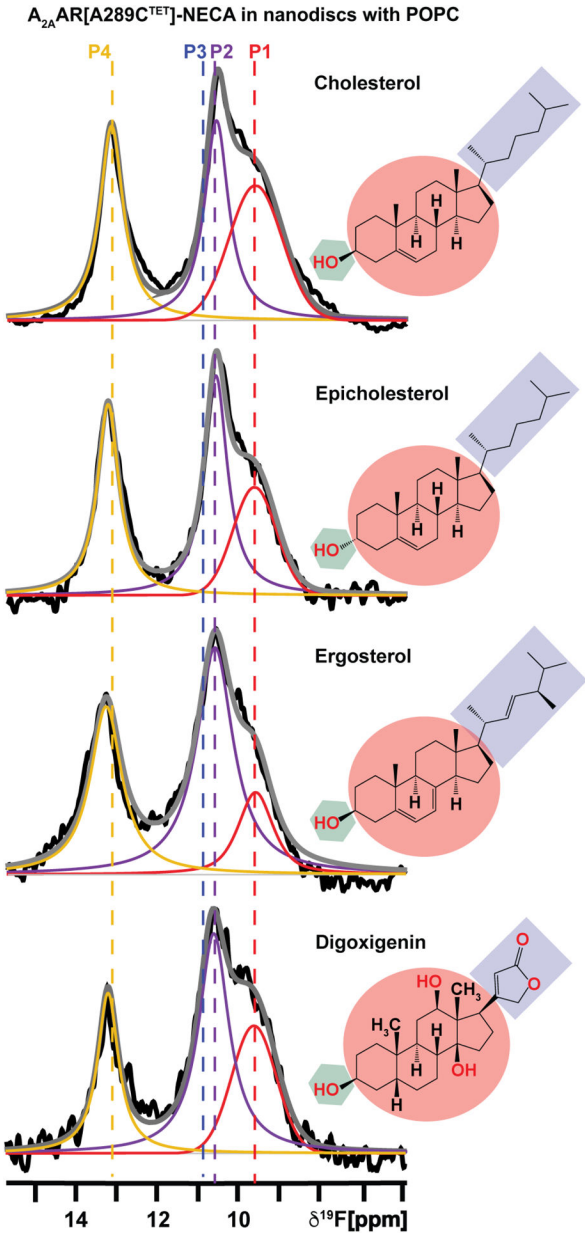

Figure 3. Sterols with different chemical structures shift the conformational equilibria of the A_{2A}AR-agonist complex toward an active ensemble.

1-dimesional ^{19}F-NMR spectra of A_{2A}AR in complex with the agonist NECA in nanodiscs containing POPC and 0.5 mol% of different sterols, as indicated. The chemical structures of each sterol are colored according to the different chemical groups. The green hexagon highlights the flexible hydroxyl head group, the maroon circle highlights the fused tetracyclic ring, and the purple box highlights the flexible iso-octyl chain of cholesterol, and the corresponding sterol analogs. Other presentation details are the same as Figure 2. See also Table S4.

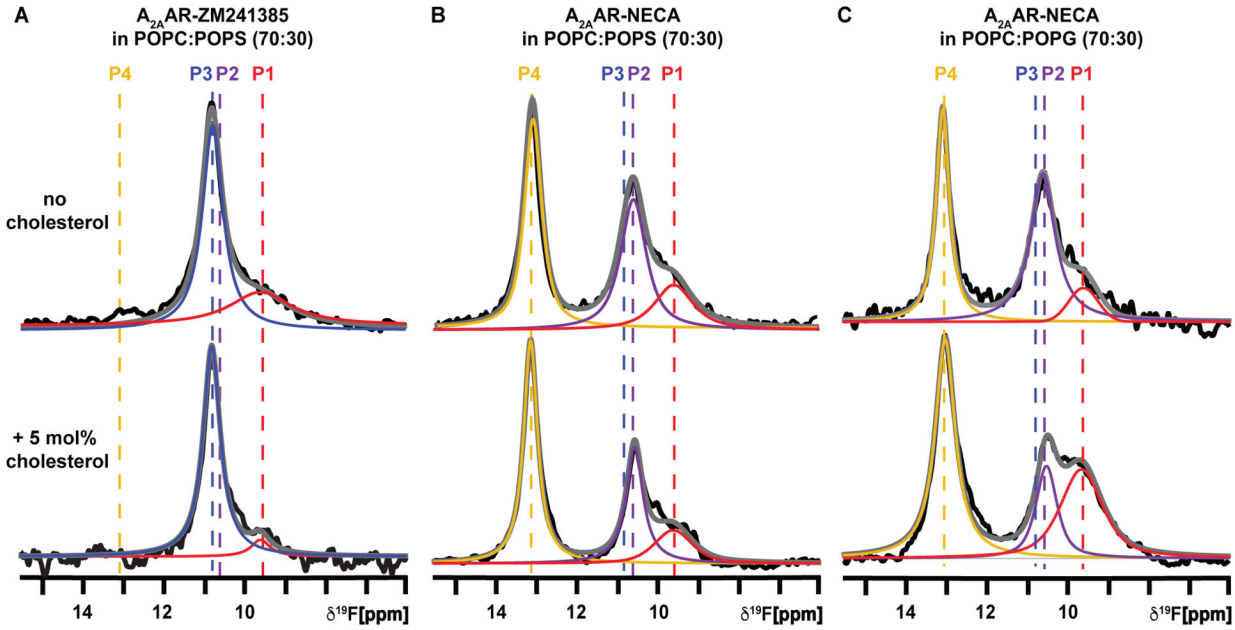

Figure 4. The presence of anionic lipids diminishes the observed impact of cholesterol on the A_{2A}AR conformational equilibria.

(A and B) The 1-dimensional ^{19}F-NMR spectra of A_{2A}AR[A289C^{TET}] in lipid nanodiscs containing POPC and POPS (70:30 molar ratio), without cholesterol or containing 5 mol% cholesterol, for complexes with (A) the antagonist ZM241385 and (B) the agonist NECA. (C) A_{2A}AR[A289C^{TET}] in lipid nanodiscs containing POPC and POPG (70:30 molar ratio), without cholesterol or with 5 mol% cholesterol, in complex with the agonist NECA. Other presentation details are the same as Figure 2. See also Figures S2, S3, S4, S10, S11, Table S3 and Table S4.

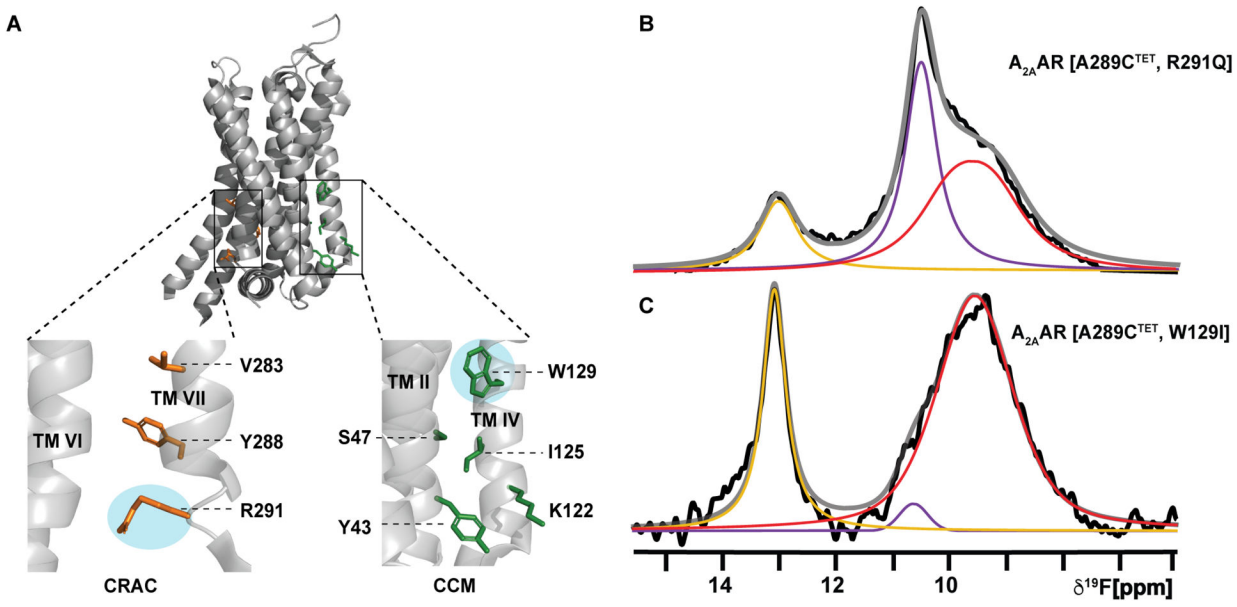

Figure 5. Impact of cholesterol interaction sites on the conformational dynamics of $A_{2A}AR$.

(A) Crystal structure of $A_{2A}AR$ (PDB: 5G53) showing the predicted CRAC site[62] (orange) and CCM site[74] (green). Expanded insets show the individual residues of each motif predicted to interact with cholesterol. Residues shown in cyan ellipses were mutated for ^{19}F NMR analysis.

(B and C) 1-dimesional ^{19}F NMR spectra of $A_{2A}AR$ variants in complexes with the agonist NECA and in nanodiscs containing POPC and 0.5 mol% cholesterol for (B) $A_{2A}AR[A289C^{TET}, R291Q]$, and (C) $A_{2A}AR[A289C^{TET}, W129I]$. Other presentation details are the same as in Figure 2. See also Table S4.

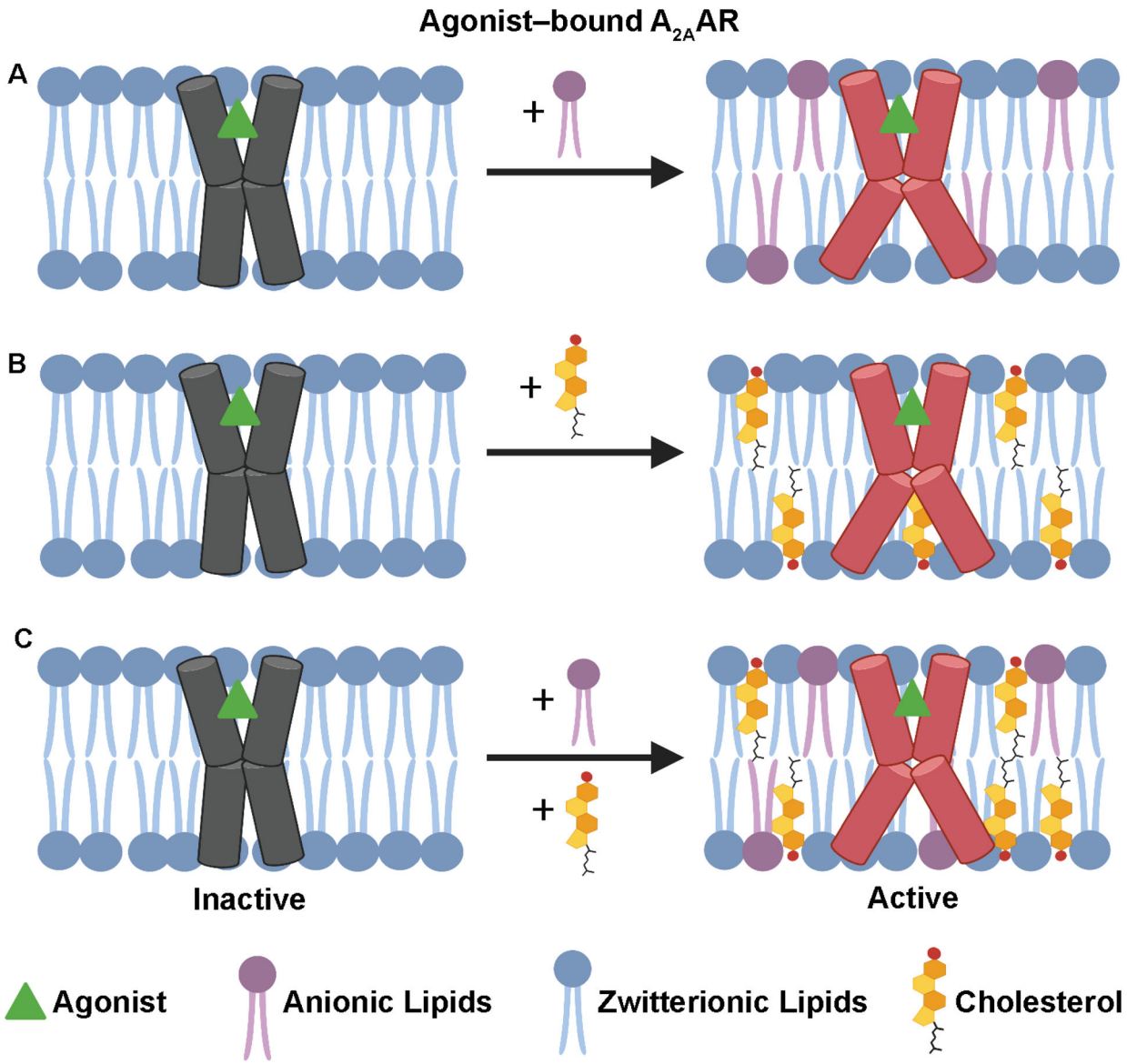

Figure 6. Visualization of the role of cholesterol on $A_{2A}AR$ function in binary and ternary lipid mixtures.

(A-C) Schematic side-views of agonist-bound $A_{2A}AR$ in phospholipid membranes illustrating the impact of adding (A) anionic lipids, (B) cholesterol, or (C) both anionic lipids and cholesterol to membranes containing zwitterionic lipids. This figure was prepared with Biorender.com.

KEY RESOURCES TABLE

REAGENT or RESOURCE	SOURCE	IDENTIFIER
Antibodies		
Monoclonal ANTI-FLAG® M2-Alkaline Phosphatase antibody produced in mouse	Sigma-Aldrich	Cat#A9469
Bacterial and virus strains		
XL10-Gold ultracompetent cells	Agilent	Cat#200314
BL21 (DE3) cells	Agilent	Cat#200132
BL21(DE3)-RIL cells	Agilent	Cat#230245
Chemicals, peptides, and recombinant proteins		
n-Dodecyl-b-D-Maltopyranoside (DDM)	Anatrace	Cat#D310
Cholesteryl hemisuccinate (CHS)	Sigma-Aldrich	Cat#C6512
Adenosine 5'-triphosphate disodium salt hydrate (ATP)	Sigma-Aldrich	Cat#34369078
4-(2-[7-Amino-2-(2-furyl)[1,2,4]triazolo[2,3-a][1,3,5]triazin-5-ylamino]ethyl)phenol (ZM241385)	Tocris	Cat#1036
5'-N-Ethylcarboxamidoadenosine (NECA)	Tocris	Cat#1691
Theophylline	Sigma-Aldrich	Cat#T1633
[3H]4-[2-[7-amino-2-(2-furyl)-1,2,4-triazolo[1,5-a][1,3,5]triazin-5-yl-amino]ethylphenol ([3H]ZM241385)	American Radiolabeled Chemicals	Cat#ART0884-50
TALON Metal Affinity Resin	Gold bio	Cat#H-310-5
Ni-NTA Metal Affinity Resin	Sigma-Aldrich	Product#70666
1-palmitoyl-2-oleoyl-glycero-3-phosphocholine (POPC)	Avanti	SKU#850457
1-palmitoyl-2-oleoyl-sn-glycero-3-phospho-L-serine (sodium salt) (POPS)	Avanti	SKU#840034
1 -palmitoyl-2-oleoyl-sn-glycero-3-phospho-(1'- rac-glycerol) (sodium salt) (POPG)	Avanti	SKU#840457
Cholic Acid, Sodium Salt	Anatrace	Cat#S1010S
Isopropyl β- d-1-thiogalactopyranoside (IPTG)	Goldbio	Cat#I2481C
Triton X-100	Sigma-Aldrich	Cat#T8787
SnakeSkin™ Dialysis Tubing, 10K MWCO, 22 mm	ThermoFischer Scientific	Cat#68100
Bio-beads SM-2 Adsorbents	BioRad	Cat#1523920
N-(2-Hydroxyethyl)piperazine-N'-(2-ethanesulfonic acid), 4-(2-Hydroxyethyl)piperazine-1-ethanesulfonic acid (HEPES)	Sigma-Aldrich	Cas#7365-45-9
TRIS Hydrochloride (Tris-HCl)	Sigma-Aldrich	Cas#1185-53-1
Ethylenediaminetetraacetic acid (EDTA)	Sigma-Aldrich	Cas#60-00-4
Cholesterol	Sigma-Aldrich	Cas#57-88-5
Ergosterol	Cayman Chemicals	Cas#57-87-4
Epi-cholesteryl methyl ether	Sigma-Aldrich	Cas#2867-93-8
Digoxigenin	Sigma-Aldrich	Cas#1672-46-4
Biotin	Sigma-Aldrich	Cas#58-85-5
Imidazole	Sigma-Aldrich	Cas#288-32-4
Glycerol	Sigma-Aldrich	Cas#56-81-5

REAGENT or RESOURCE	SOURCE	IDENTIFIER
Sodium phosphate monobasic anhydrous	Sigma-Aldrich	Cas#7558-80-7
Sodium phosphate dibasic anhydrous	Sigma-Aldrich	Cas#7558-79-4
Magnesium Chloride	Sigma-Aldrich	Cas#7791-18-6
Methanol	Sigma-Aldrich	Cas#67-56-1
DMSO	Fisher Scientific	Cas#67-68-5
Sodium Chloride	Sigma-Aldrich	Cas#7647-14-5
Potassium Chloride	Sigma-Aldrich	Cas#7447-40-7
Aldrithiol-4	Sigma-Aldrich	Cas#2645-22-9
2,2,2-Trifluoroethanethiol (TET)	Sigma-Aldrich	Cas#1544-53-2
Trifluoroacetic acid (TFA)	Sigma-Aldrich	Cas#76051
N-[4-(7-diethylamino-4-methyl-3-coumarinyl)phenyl]maleimide (CPM)	Invitrogen	Cat#D346
Guanosine-5'-diphosphate (disodium salt) (GDP)	ThermoFisher Scientific	Cas#7415-69-2
2-Iodoacetamide	TCI Chemicals	Cas#144-48-9
Laurdan	Tocris	Cas#74515-25-6
Deposited data		
A_{2A}AR in complex with ZM241385	Jaakola et al., 2008[46]	PDB: 3EML
A_{2A}AR in complex with NECA bound to an engineered G protein	Carpenter et al., 2016[44]	PDB:5G53
Experimental models: Organisms/strains		
P. pastoris: Bg12	BioGrammatics	Cat#PS004-01
Oligonucleotides		
A_{2A}AR[A289C,W129I] Forward: [5'AAGGGCATCATTGCCATCTGCATTGTGCTGTCGIIIGCCATCGGCCTGAC3']	This study	n/a
A_{2A}AR[A289C,W129I] Reverse: [5'GTCAGGCCGATGGCAAACGACAGCACAATGCAGATGGCAATGATGCCCTT3']	This study	n/a
Recombinant DNA		
Plasmid: human A_{2A}AR (1-316) in pPIC9K	Eddy et al., 2018[50]	n/a
Plasmid: human A_{2A}AR[A289C]	Thakur et al., 202364	n/a
Plasmid: human A_{2A}AR[A289C,R291Q]	Thakur et al., 202364	n/a
Software and algorithms		
GraphPad prism	GraphPad Software Inc.	https://www.graphpad.com
MestreNova 14.1.1-24571	MestreLab Research S.L	https://mestrelab.com/download/mnova/
Topspin 4.0.8	Bruker Biospin	https://www.bruker.com/en/products-and-solutions/mr/nmr-software/topspin.html

REAGENT or RESOURCE	SOURCE	IDENTIFIER
UCSF Chimera	UCSF	https://www.cgLucsf.edu/chimera/
Other		
PD-10 column	Cytiva	Cat#17085101
Vivaspin® 6 ultrafiltration spin columns MWCO 30 kDa	Cytiva	Cat#28932361
Vivaspin® 6 ultrafiltration spin columns MWCO 10 kDa	Sigma-Aldrich	SKU#GE28932296
AccuPrime Pfx SuperMix	ThermoFischer Scientific	Cat#12344040
SnakeSkin™ Dialysis Tubing, 10K MWCO, 22 mm	ThermoFischer Scientific	Cat#68100
Amplex Red Cholesterol Assay Kit	ThermoFischer Scientific	Cat#A12216
GTPase-Glo Assay	Promega	Cat#V7681